

# **Suspended Micro/ nanofiber Hierarchical Scaffolds for Studying Cell Mechanobiology**

Ji Wang

Thesis submitted to the faculty of the Virginia Polytechnic Institute and State University in partial fulfillment of the requirements for the degree of  
Master of Science  
In  
Macromolecular Science and Engineering

Amrinder S. Nain, Chair

Judy S. Riffle

S. Richard Turner

February 11<sup>th</sup>, 2015

Blacksburg, Virginia

Key words: nanofiber manufacturing, hierarchical scaffolds, cell geometry, single cell forces

# Suspended Micro/ nanofiber Hierarchical Scaffolds for Studying Cell Mechanobiology

Ji Wang

## Abstract

Extracellular matrix (ECM) is a fibrous natural cell environment, possessing complicated micro- and nano- architectures, which provides signaling cues and influences cell behavior. Mimicking this three dimensional environment *in vitro* is a challenge in developmental and disease biology. Here, suspended multilayer hierarchical nanofiber assemblies fabricated using the non-electrospinning STEP (Spinneret based Tunable Engineered Parameter) fiber manufacturing technique with controlled fiber diameter (microns to less than 100 nm), orientation and spacing in single and multiple layers are demonstrated as biological scaffolds.

Hierarchical nanofiber assemblies were developed to control single cell shape (shape index from 0.15 to 0.57), nuclei shape (shape index 0.75 to 0.99) and focal adhesion cluster length (8-15 micrometer). To further investigate single cell-ECM biophysical interactions, nanofiber nets fused in crisscross patterns were manufactured to measure the “inside out” contractile forces of single mesenchymal stem cells (MSCs). The contractile forces (18-320 nano Newton) were found to scale with fiber structural stiffness (2-100 nano Newton/micrometer). Cells were observed to shed debris on fibers, which were found to exert forces (15-20 nano Newton). Upon CO<sub>2</sub> deprivation, cells were observed to monotonically reduce cell spread area and contractile forces. During the apoptotic process, cells exerted both expansive and contractile forces. The platform developed in this study allows a wide parametric investigation of biophysical cues which influence cell behaviors with implications in tissue engineering, developmental biology, and disease biology.

## **Acknowledgement**

I'd like to express my gratitude to the people that made this work possible and provided guidance over my time at Virginia Tech. My advisor, Professor Amrinder Nain for welcoming me as the first student into his team, providing guidance and encouragement throughout the whole process, and for allowing the freedom to explore interesting topics as they came up, regardless of the outcome. Additionally, I'd like to thank the rest of my committee, Professor Judy Riffle and Professor Richard Turner for their guidance and encouragement both in class and in the context of my research. I'd like to thank Virginia tech and the Macromolecules and Interfaces Institute for providing funding and support, and ICTAS and the NCFL facilities and equipment. I would also like to thank other members in the STEP lab for their suggestions and collaboration. My work would not have been possible without the support of Kevin Sheets, Puja Sharma, Colin Ng, Brian Koons , Amritpal Gil and the rest of the STEP lab. Additionally, I'd like to thank Dr. Behkam's group for their sincere and generous help. I wish all of you good luck in your work in the future, wherever it leads you. I acknowledge the financial support from Biomedical Engineering and Mechanics Department and Macromolecules and Interfaces Institute during this study.

## Table of Content

<b>Chapter 1 Introduction</b> .....	1
<b>1.1 Motivations</b> .....	1
<b>1.2 A Brief Survey of Current Continuous Polymer Nanofiber Fabrication Approaches</b> .....	3
<b>1.3 Focus of This Work</b> .....	5
<b>Chapter 2 Materials and Methods</b> .....	7
<b>2.1 Polymer Solution Preparation</b> .....	7
<b>2.2 STEP Spinning</b> .....	7
<b>2.3 Cell Culturing</b> .....	7
<b>2.4 Fluorescence Microscopy</b> .....	8
<b>2.5 AFM based Stiffness Measurement</b> .....	8
<b>2.6 SEM Characterization</b> .....	9
<b>2.7 Statistical Methods</b> .....	9
<b>Chapter 3 Results and Discussion</b> .....	10
<b>3.1 Non-electrospinning STEP Technique</b> .....	10
<b>3.2 Suspended Micro/Nanofiber Hierarchical Biological Scaffolds</b> .....	13
<b>3.3 Contractile Cell Force Probes using Suspended Nanofiber Networks</b> .....	23
<b>3.3.1 Fabrication and Characterization of Nanofiber Nets</b> .....	23
<b>3.3.2 Mesenchymal Stem Cell Contractile Force Measurement based on Nanofiber Nets</b> .....	30
<b>Chapter 4 Conclusions and Future Work</b> .....	36
<b>References</b> .....	38
<b>Appendix A: Copy Right Permission from Langmuir</b> .....	44
<b>Appendix B: Copy Right Permission from Polymer Journal Nature</b> .....	45

## List of Figures

<b>Figure 1:</b> (A) Schematic illustration of STEP, (B) PS fiber diameters as a function of substrate rotating speed ' $\omega$ ' for 2000K (g.mol <sup>-1</sup> ) PS 65.1mg.ml <sup>-1</sup> solution in p-xylene. (C-F) 3-D STEP fiber collections on cube, cylinder, sphere and shape assemblies respectively. ....	10
<b>Figure 2:</b> Schematic illustration of fiber formation process in STEP process. ....	11
<b>Figure 3:</b> Crisscrossed STEP fibers made from varied polymer species. polystyrene (PS) (A), poly (methyl methacrylate) (PMMA) (B) and fibrinogen (C) respectively. Scale bars represent 1 $\mu$ m in inserts of A and C. ....	12
<b>Figure 4:</b> STEP capability in achieving control in single and double layer structures. (A-D) Arrays of 8000, 500, 150 and 30nm diameter PS fibers, (E) relative angles between adjacent fibers, (F) fiber spacing variation. ....	14
<b>Figure 5:</b> Bottom up PS nanofiber assemblies using STEP :(A) 70nm fiber arrays on top of a 800nm diameter fiber,(B) 800nm diameter fiber arrays in orthogonal configurations,(C) three layers of fiber arrays configured at 60° angles with each other with $d_1=d_2=400$ nm, $d_3=800$ nm, (D) a hierarchical fiber assembly of different diameter fibers with controlled orientations $d_1=400$ nm, $d_2=800$ nm, $d_3=d_4=70$ nm; $\alpha_{12}=\alpha_{23}=80^\circ, \alpha_{34}=90^\circ$ . ....	16
<b>Figure 6:</b> Schematic and SEM images of partial section of six layer bottom up hierarchical assembly with numbers denoting the bottom up sequence of deposition. Highlighted frames in inserts I-III are PS, PMMA and PU unit cells respectively. Insert IV and V demonstrates the bottom up deposition sequence. Scale bars represent 10 $\mu$ m in inserts I-V. ....	18
<b>Figure 7:</b> (A)-(D) Representative fluorescent images of C2C12 mouse myoblasts on divergent fibers with varying angles (A) 0°, (B) 30°, (C) 60°, (D) 90°, (E-F) cell shape index and cell spread area as a function of divergent angles $\pm$ SE. * shows statistical significance ( $P<0.01, n=60$ /category). Scale bars represent 20 $\mu$ m in (A)-(D). ....	19
<b>Figure 8:</b> (A)-(D) Representative focal adhesion paxillin (green) and nucleus (blue) images of C2C12 mouse myoblasts on SL, SS, DL and DS hierarchical architectures, (E) FAC cluster length, and (F) cell nucleus shape index of C2C12 mouse myoblasts on four conformation of hierarchical architectures $\pm$ SE. * shows statistical significance ( $P<0.05, n=50$ /category). ....	21
<b>Figure 9:</b> (A) Schematic illustration of SEM images of suspended STEP nanofiber nets. (B) SEM image of an orthogonal patterns of bigger and smaller diameter fibers.....	23
<b>Figure 10:</b> (A) Illustration of a suspended nanofiber deflected by an AFM cantilever. (B) A force vs deflection curve of a single suspended PS nanofiber. ....	26
<b>Figure 11:</b> Product of apparent stiffness $k_{app}$ and $L/D^2$ of PS nanofibers as a function of $(D/L)^2$ .....	27
<b>Figure 12:</b> (A) A schematic illustration of a “tie rod” model for cell contractile force calculation. (B) A fluorescent cell image showing the “inside out” cell force measurement. ....	28
<b>Figure 13:</b> Stiffness variation along the length of a suspended fiber with 200nm diameter and 320 $\mu$ m length. Yellow dots represent the experimental value obtained by deflecting the fiber at different locations using an AFM cantilever. ....	29
<b>Figure 14:</b> (A) Single fiber deflection with $L=230$ mm, $d=300$ nm, $\Theta=40^\circ$ , $P_1=18$ nN, $P_2=22$ nN, fiber stiffness 6nN/ $\square$ m. (B) Single fiber deflection with $L=120$ mm, $d=800$ nm, $\Theta=40^\circ$ , $P_1=150$ nN, $P_2=131$ nN, fiber stiffness 82 nN/ $\square$ m. (C) MSC contractile forces as a function of local stiffness, $N=60$ . ....	31
<b>Figure 15:</b> (A) Time lapse of a MSC migration along two parallel fibers. Scale bars represent 5 $\mu$ m. (B) Time evolution of the force exerted by the leading edge and trailing edge. (C) Trailing and (D) leading edge force evolution along fiber length in conjunction with stiffness variation edge. Scale bar represent 20 $\mu$ m. ....	32

**Figure 16:** (A) Time lapse of a MSC debris deflecting nanofiber nets. (B) Contractile force evolution of the MSC debris. (C) Mesenchymal stem cell and debris contractile force as a function of local stiffness. Scale bar represent 20  $\mu\text{m}$ . ..... 33

**Figure 17:** (A) (B) Time lapse of a MSC undergoing CO<sub>2</sub> deprivation. (C) Cell area reduction and contractile force evolution during CO<sub>2</sub> deprivation process. .... 34

**Figure 18:** Mesenchymal stem cell forces evolution during apoptosis. (A)-(C) Time lapse images corresponding to three stages of apoptosis. (D) Expanding and contracting forces during the cell apoptosis process. .... 35

**List of Tables**

Table 1 PS fiber diameters as a function of solvent, solution concentration and molecular weight. .... 12  
Table 2 Control of fiber spacing at  $\omega=40$  rPS by manipulating  $V_t$ . .... 13  
Table 3 Mechanical Properties of single PS nanofibers..... 27

**List of Equations**

Equation 1 ..... 25  
Equation 2 ..... 25  
Equation 3 ..... 25  
Equation 4 ..... 27  
Equation 5 ..... 28  
Equation 6 ..... 29



## List of Abbreviations

STEP	Spinneret based Tunable Engineered Parameter
ECM	Extracellular matrix
MSC	Mesenchymal Stem Cell
nm	Nano meter
nN	Nano Newton
μm	Micro meter
mm	Millimeter
AFM	Atomic Force Microscope
PS	Polystyrene
PMMA	Poly methyl methacrylate
PU	Poly Urethane
DC	Direct Current
RPS	Rotation Per Second
ml	Milliliter
μl	Microliter
μg	Microgram
SEM	Scanning Electron Microscope
FAC	Focal Adhesion Cluster
SI	Shape Index

# Chapter 1 Introduction

## 1.1 Motivations

Cell behavior is directly affected by extracellular matrix (ECM), which is primarily composed of natural hierarchical assemblies of protein nanofibers.[1–3] The hierarchical architecture of the surrounding ECM is comprised of individual fibrous proteins (30-70 nm diameter), which can form bundles (100nm-microns in diameter).[4–10] These bundles of fibers are observed to be aligned or seemingly randomly distributed *in vivo*. [11–14] Due to imaging limitations *in vivo*, much of our current understanding about fundamental cell processes is derived from reductionist *in vitro* platforms, such as flat substrates and gels, which aim to capture a complete *in vivo* description replete with simultaneous biophysical and biochemical cues.[15–17]. In this regard, significant work has been done to develop *in vitro* platforms. As an example, micro-patterned flat surface approaches involve micro-fabrication of cell-adhesive patches on cell culture substrates with high precision using soft lithography or photolithography.[18,19] The engineered surfaces with the ability to constrain cell spreading to a specific cell-surface area have been shown to dramatically affect cell proliferation, differentiation, migration and apoptosis.[20,21] However, the complexity in preparation of the cell-adhering substrates coupled with their long term stability and compatibility in cell-culture medium are typical problems requiring consideration. [22,23] On the other hand, hydrogel-crosslinked networks possessing high water content have been intensively utilized for *in vitro* cell experiments.[24] Cells embedded into hydrogels sense confinement from both mechanical properties of the hydrogels and pericellular accumulation of ECM proteins. However, tuning the mechanical properties of hydrogels can be difficult as it involves a complex interplay of network properties, swelling characteristics, degradation rates and deposition of ECM macromolecules.[25] While these platforms have indeed provided a deeper

understanding of cell-substrate interactions and mechanotransduction, interpretation from a cell-ECM perspective is still challenging since these 2D and 3D structures are unable to capture features of *in vivo* fibrous ECM, such as fiber alignment, diameter (curvature) and structure bending stiffness (N/m).

Recently, nanofiber assemblies have been studied as bioassays providing 3D topology that better mimics the architectures formed by fibrous ECM proteins. It is well known that besides chemical composition and morphology of individual nanofibers, nanofiber orientation plays important roles in guiding cellular responses.[26,27] Ramakrishna *et al.* collected aligned polymer nanofibers on a rotating drum collector for vascular tissue engineering and they found that human coronary artery muscle cells express a spindle-like shape and the cytoskeleton inside these cells was parallel to the direction of the nanofibers.[28,29] Yang *et al.* seeded neural stem cells (NSCs) on aligned PLLA nanofiber scaffolds and they found that the direction of NSC elongation and outgrowth was parallel to the fibers and the NSC differentiation was higher on PLLA nanofibers than that on micro fibers.[30] Lee *et al.* found that human ligament fibroblasts (HLF) on the aligned nanofibers were spindle-shaped and synthesized significantly more collagen than those on random nanofiber sheets.[31]

Suspended nanofibers possessing diameters closely resembling those of the native fibrous ECM proteins provide a curved surface for cell attachment and have mechanical properties that can be tuned to investigate biophysical influence on cell behaviors. Using suspended nanofiber assemblies as a platform, Nain *et al.* demonstrated that cells on aligned and suspended fibers exhibited higher migration speeds and changes in migration direction in the direction of diverging

fibers [32]. Recently, work by Sheets *et al.* has demonstrated that cells on suspended fibers have focal adhesion cluster length ~4X longer than those on flat substrates, which may be the reason why cells have different behaviors associated with fiber dimensionality.[33] In the context of disease models, Sharma *et al.* has demonstrated that the bleb size and number density of blebs on a cell inversely correlates with the area, with blebs on glioma cells eliminated at a cell spread area of ~1600  $\mu\text{m}^2$ . [8]

The suspended nanofibers cause cells to react to surface curvature and dimensionality that flat substrates inherently mask, thus providing a unique platform for investigating cell-fiber interactions. We speculate that the topological parameters (fiber diameter and alignment) along with the structural stiffness in suspended nanofiber assemblies elicits diverse cell behaviors as measured by a large number of metrics, including cell shape and area, nucleus shape index, focal adhesion cluster (FAC) length and cell contraction forces.

## **1.2 A Brief Survey of Current Continuous Polymer Nanofiber Fabrication Approaches**

*In vitro* culture conditions mimicking fibrous ECM mechanics/topography have tremendous potential for studying cellular behaviors for applications in tissue engineering and has been a target for multiple nanofabrication techniques, such as nanolithography, micro/nano printing and electrospinning technique.[34,35] Key factors impacting fiber use in cell studies include the ability to precisely control fiber diameter and deposition (orientation and spacing). The recent advancements in achieving control of fiber deposition include electrospinning (far-field electrospinning (FFES), near-field electrospinning (NFES)) and direct drawing.

Electrospinning is the most widely known method of forming continuous polymeric nanofibers. In this process, polymer solution is pumped through a needle where an electric field extrudes polymer fibers on a collecting target. In the past decade, the bioengineering community has seen rapid growth in the use and improvement of electrospinning techniques to achieve nanofiber scaffolds with control of fiber diameter and alignment. To create aligned nanofiber assemblies, a high speed rotating drum or patterned electrodes are commonly used as a collector. In this regard, Li *et al.* have demonstrated fabrication of aligned electrospun nanofibers using patterned electrodes,[36] Katta *et al.* demonstrated aligned electrospun nanofibers on a high speed rotating drum,[37] and Zussman *et al.* fabricated nanofiber arrays and crisscross patterns using a wheel-like bobbin collector.[38,39] Similarly Teo *et al.* collected aligned nanofibers by placing two blades in line with one another with a gap between them.[40] Dalton *et al.* used two rings placed in parallel to collect highly aligned fibers that were deposited at the perimeters of the rings. [41] Although a certain degree of fiber alignment has been achieved, these approaches have encountered difficulties in spatially arranging fibers with accurately controlled diameter and spacing due to the inherent electric instabilities.

On the other hand, NFES has demonstrated improved fiber patterning through reducing applied voltage and the source-to-target distance. Bisht *et al.* deposited aligned polymeric nanofibers on three dimensional substrates using low voltage (200 V) near-field electrospinning.[42] Sun *et al.* demonstrated orderly collected nanofibers by using a 600 V voltage and a source-to-target distances ~10mm. [43] The bending instabilities are reduced, resulting in better control of the

polymer solution jet. However, precise multilayer fiber patterning on large surfaces using NFES has yet to be demonstrated.

In contrast, direct drawing method using polymer wetted probe tips has recently demonstrated precise micro/nanofiber depositions. Nain *et al.* used proximal probes (AFM cantilevers and glass micropipettes) to draw polymer fibers down to a few hundred nanofibers in diameter and several hundred micrometers in length.[44,45] Although well-organized fiber patterns have been demonstrated, it is unclear if this approach can be extended to build large area multi-layer nanofiber assemblies given the short operating time available under solvent evaporation.

### **1.3 Focus of This Work**

In this work, we utilize Spinneret based Tunable Engineered Parameters (STEP) technique to manufacture suspended and aligned nanofiber assemblies to investigate cellular behaviors. The STEP technique allows accurate deposition of suspended and aligned polymeric nanofibers whose diameter are in the range of fibrous ECM proteins, thus creating an *in vitro* platform that topographically represents the microenvironment of cells. Based on this platform, our research includes:

1. We developed hierarchical nanofiber assemblies using STEP technique. Using aligned nanofibers as substrates, we investigated the single cell arrangement at high magnifications, specifically, we explored of the influence of biophysical cues on C2C12 mouse myoblasts behaviors, including cell geometry, nucleus shape index and focal adhesion cluster length.

2. We measured the contractile forces of cells attached to suspended fibers. Mesenchymal stem cell contractile forces are measured based on suspended and aligned nanonets during cell migration and the apoptosis process.

## Chapter 2 Materials and Methods

### 2.1 Polymer Solution Preparation

All chemicals were used as received without further purification. Polystyrene (PS) of several molecular weights ( $M_w$ ) (860K, 1500K, and 2000K  $\text{g}\cdot\text{mol}^{-1}$ , Polymer Scientific, USA) were dissolved at room temperature in *p*-xylene and tetrahydrofuran (THF) at varying concentrations for one week prior to experiments. Poly(methyl methacrylate) (PMMA,  $M_w = 540\text{K}$   $\text{g}\cdot\text{mol}^{-1}$ , Polymer scientific, USA) was dissolved in chlorobenzene at  $134 \text{ mg}\cdot\text{ml}^{-1}$ , and the polyurethane (PU5719, Lubrizol Advanced Material, USA) was dissolved in DMF at  $292 \text{ mg}\cdot\text{ml}^{-1}$ . Bovine fibrinogen fraction 1 from plasma (340 kDa, Sigma-Aldrich Chemical Co., USA) was dissolved in HFP at  $100 \text{ mg}\cdot\text{ml}^{-1}$ .

### 2.2 STEP Spinning

The viscous polymer solutions were pumped through the 100 micron diameter micropipette spinneret (Jensen Global, USA). The substrate was mounted onto a DC motor, which in turn was mounted onto a motorized three degree of freedom micro-positioning stage (VP-25XA, Newport Inc, USA). No voltage source was used in the experiments to eject polymer solution.

### 2.3 Cell Culturing

STEP scaffolds were mounted on glass-bottom six-well plates (MatTek Corp., Ashland, MA). Fiber scaffolds were sterilized by adding 2 ml of 70% ethanol for 10 min, then coated with  $2\mu\text{g}\cdot\text{ml}^{-1}$  fibronectin (Invitrogen, Carlsbad, CA).[8,33] C2C12 mouse myoblasts (American Type Culture Collection, Manassas, VA) were cultured in Dulbecco's Modified Eagle Medium (DMEM)



supplemented with 10% fetal bovine serum (FBS) and 1% penicillin/streptomycin (HyClone Laboratories, Logan, UT). Cells were seeded onto the fiber scaffolds via 30  $\mu\text{l}$  droplets at a concentration of 100,000 cells  $\text{ml}^{-1}$  and incubated at 37 °C and 5%  $\text{CO}_2$ . Cells were then given 2–6 h to attach onto the nanofibers. After 1 hour of seeding, 2 ml of medium was added to each well.

## **2. 4 Fluorescence Microscopy**

F-actin stress fibers, focal adhesions and the nucleus in C2C12 mouse myoblasts were stained. Cells were fixed in 4% paraformaldehyde, permeabilized in a 0.1% Triton X100 solution and blocked in 10% goat serum. Primary goat antipaxillin antibodies (Invitrogen) were diluted 1:250 and incubated at 4 C° for 1 h. Secondary goat anti-rabbit antibodies conjugated to Alexa Fluor 488 (Invitrogen) were then added along with a 1:100 dilution of rhodamine phalloidin (Santa Cruz Biotechnology, Santa Cruz, CA) and placed at room temperature for 45 min and protected from light. DAPI counterstaining was performed by adding 300 nM DAPI (Invitrogen) for 5 min. The substrates were then rinsed with PBS and observed using a Zeiss microscope. Fiber scaffolds were kept hydrated in 1 ml phosphate buffered saline (PBS) during imaging.

## **2.5 AFM based Stiffness Measurement**

Nanofiber stiffness was measured by deflecting the suspended nanofiber at the middle using an AFM cantilever (DNP S-10 cantilevers of stiffness 0.175–0.7  $\text{Nm}^{-1}$ , Bruker, California) The measurements were made in contact mode, and the stiffness of the cantilever was measured every time before use.

## **2.6 SEM Characterization**

For SEM (Zeiss, Leo 1550) analysis, the samples were placed on gold-coated stubs and sputter coated.

## **2.7 Statistical Methods**

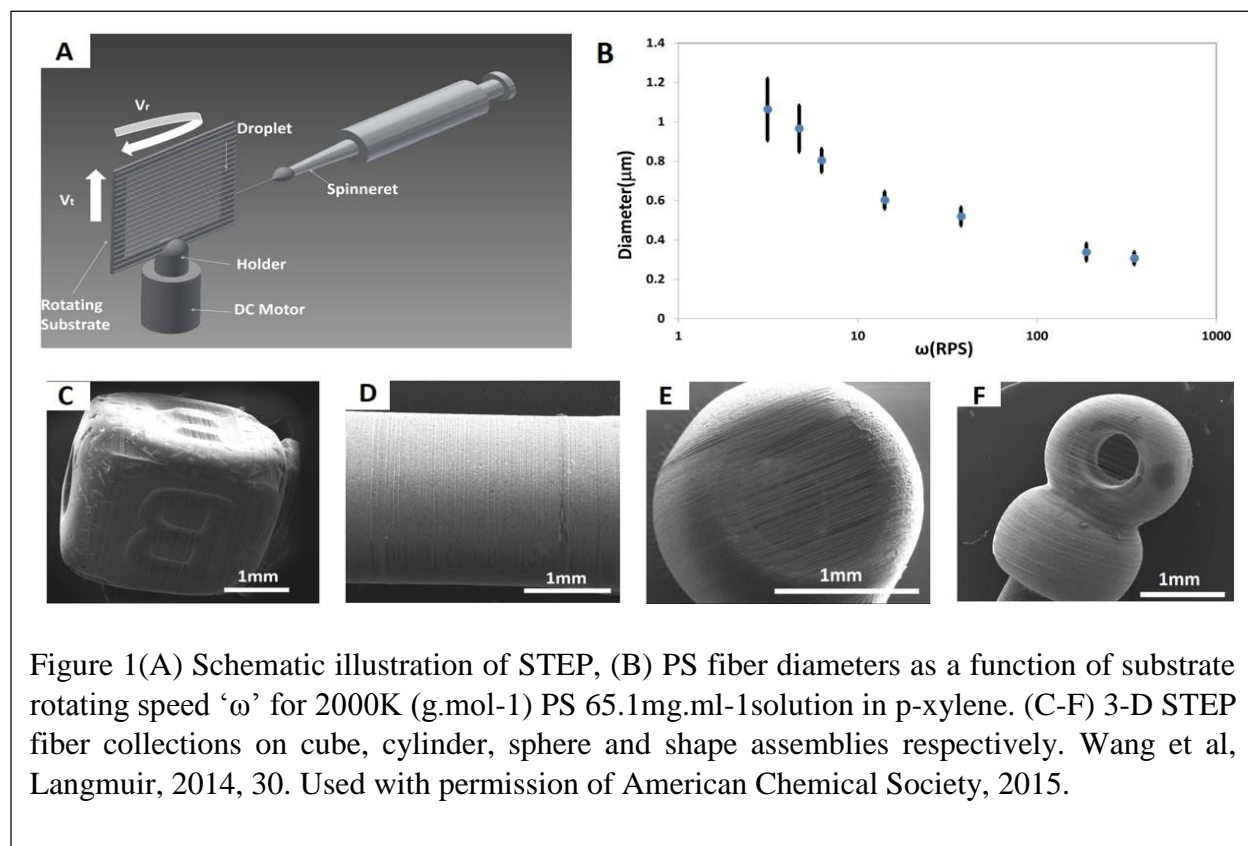
Statistical analysis and graphing were performed using GraphPad software. One way ANOVA testing with Tukey post testing comparing all pairs of data sets was performed. Bar graphs are presented with standard error bars.

**Note:** Cell culturing and fluorescence microscopy were conducted by Kevin Sheets and Puja Sharma.

## Chapter 3 Results and Discussion

### 3.1 Non-electrospinning STEP Technique

In a typical STEP fiber fabrication process, polymer solution is extruded from a micropipette and forms a droplet (Figure 1(A)). The droplet is brought in contact with a rotating substrate mounted onto a three degree of freedom micro-positioning stage. Thus, in this set up, the substrate undergoes both rotational ( $V_r$ ) and translational ( $V_t$ ) motions. As the rotating substrate translates vertically, a polymeric filament is continuously extracted from the solution droplet and subsequently deposited on the substrate in parallel configurations. Controlled fiber deposition on various shapes (cube, cylinder, sphere, and shape assemblies) makes STEP an attractive technique for achieving fiber assemblies on curved surfaces of varying geometries (Figure 1(C-F)).[46] STEP fiber formation depends on material and processing parameters. Fiber diameter scales with



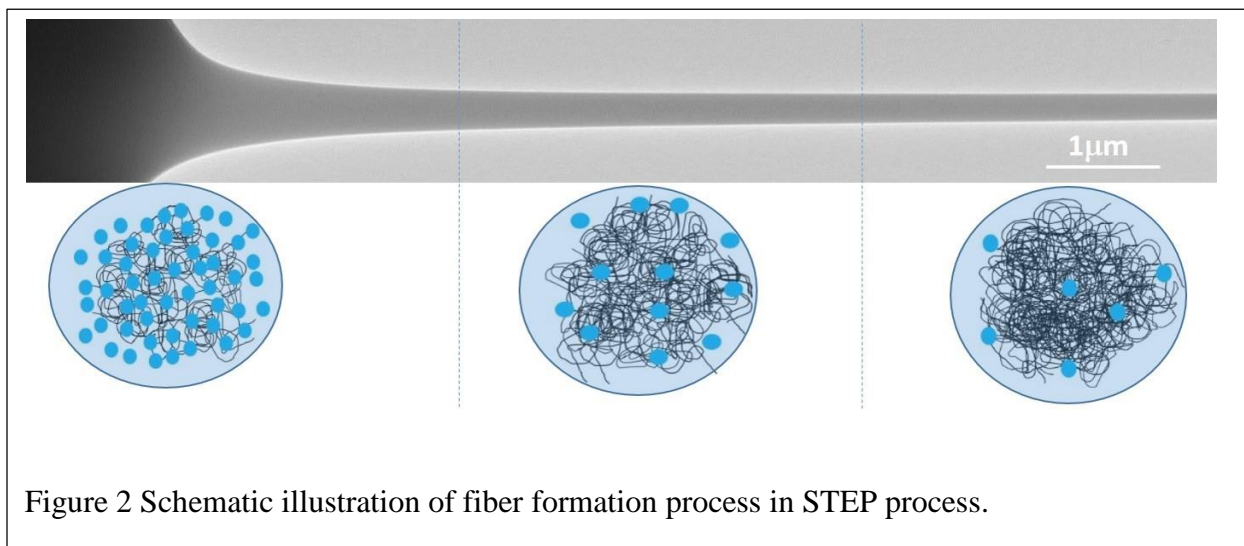


Figure 2 Schematic illustration of fiber formation process in STEP process.

rotational speed ( $\omega$ ) as shown in Figure 1(B), and in this study, all fibers were obtained at a constant rotating speed  $\omega=40$  *rPS* (substrate width=8 mm).

Smooth and uniform diameter fibers start to form as the solution concentrations approach critical entanglement concentration  $C_e$ , which signify sufficient number of polymer chain entanglements leading to a long range of elastic network required for fiber formation.[47] Fiber diameter was controlled through a combination of material parameters, including solvent volatility (e.g. boiling point), solution concentration and molecular weight of the polymer. Higher solution concentration, low boiling point solvent and higher molecular weight lead to less deformable entangled polymer chain networks (Figure 2), thus producing larger fiber diameters. Using these approaches, we have been able to control fiber diameters in a fairly large range from 30 nm to 8  $\mu$ m (Table 1). Note that the diameter of fibrous ECM proteins ranges from 50 nm (e.g. collagen fibrils) to microns (e.g. collagen fiber bundles), which is well within the diameter range of STEP fibers.[48] Therefore, it is possible to topographically mimic native ECM at different scales using STEP fibers.

Table 1 PS fiber diameters as a function of solvent, solution concentration and molecular weight. Wang et al, Langmuir, 2014, 30. Used with permission of American Chemical Society, 2015.

Concentration (mg.ml <sup>-1</sup> )	Molecular Weight (g.mol <sup>-1</sup> )	Solvent	Diameter(nm) <sub>[a]</sub>
127	2000K	THF	8067±881
63	2000K	THF	3621±361
63	1500K	THF	2376±213
65	2000K	<i>P</i> -xylene	520±42
36	1500K	<i>P</i> -xylene	139±14
55	860K	<i>P</i> -xylene	34±4

[a]Fiber diameter was averaged over at least 50 measurements.

By choosing an appropriate rotational substrate speed and vertical translation of the substrate, scaffolds with parallel fibers and crisscrossed fibers are fabricated. In addition, suspended nanofibers can be achieved by depositing fibers on a hollowed-out support base. (Figure 3) Using

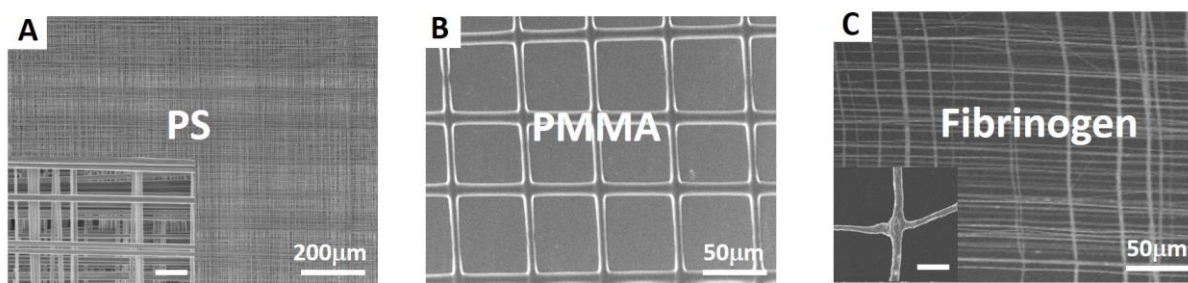


Figure 3 Crisscrossed STEP fibers made from varied polymer species. polystyrene (PS) (A), poly (methyl methacrylate) (PMMA) (B) and fibrinogen (C) respectively. Scale bars represent 1 μm in inserts of A and C. Wang et al, Langmuir, 2014, 30. Used with permission of American Chemical Society, 2015.

this technique, we have obtained aligned micro/nanofibers from various polymer species, including polystyrene (PS), poly(methyl methacrylate) (PMMA), poly(ethylene oxide) (PEO), and fibrinogen fibers.

### 3.2 Suspended Micro/Nanofiber Hierarchical Biological Scaffolds

Table 2 Control of fiber spacing at  $\omega=40$  rPS by manipulating  $V_t$ . Wang et al, Langmuir, 2014, 30. Used with permission of American Chemical Society, 2015.

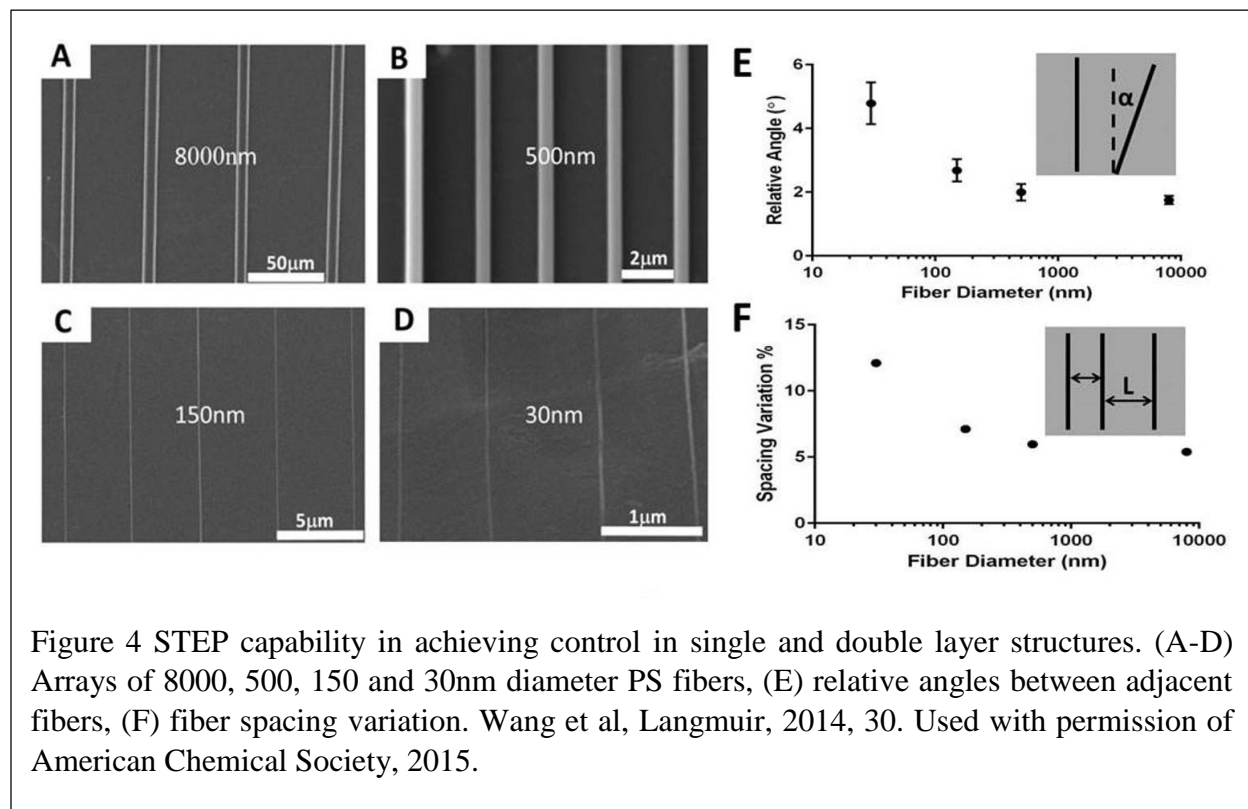
Fiber Diameter (nm)	Desired Spacing ( $\mu\text{m}$ )	$V_t$ (mm/s)	Average Spacing ( $\mu\text{m}$ ) <sub>[a]</sub>
8000	50	2.27	53.2
500	2	0.11	1.8
150	5	0.20	4.7
30	1	0.04	1.1

[a]Fiber spacing was averaged over 30 measurements in fiber arrays.

STEP based fiber manufacturing provides a single stable filament from the pendant droplet, leading to uniform diameter fibers which can be deposited precisely in ordered configurations, thus enabling accurate control of fiber diameter, alignment and spacing. As no solution filament spraying or branching occurs during STEP fabrication, the fiber diameter variation is well controlled within 12%. (Table 1). In addition, since the filament is directly pulled out from the solution droplet by the collecting substrate, the source-to-target distance, where instability is typically found in electrospinning, is absent. The absence of filament whipping in STEP results in a very high degree of alignment, where relative angles between fibers in an array are maintained less than  $3^\circ$  for microfiber and less than  $6^\circ$  for sub 100 nm diameter fibers (Figure 4(A-E)). Furthermore, STEP technique allows patterning ultrathin nanofibers of 30 nm in diameter (Figure 4(D)), which is comparable to the lowest diameter that can be aligned with

electrospinning.[38,49,50] To achieve desired fiber spacing, the required translation speed  $V_t$  (mm/s) of the substrate is easily estimated by:  $V_t = d \times RPS + L \times (RPS-1)$ , where  $d$  is the fiber diameter and  $L$  is the desired fiber spacing. (Table 2). Using this, the average fiber spacing variation was maintained less than 7% for micro and 15% for nanoscale fiber arrays as shown in Figure 4(A-D) and (F).[46]

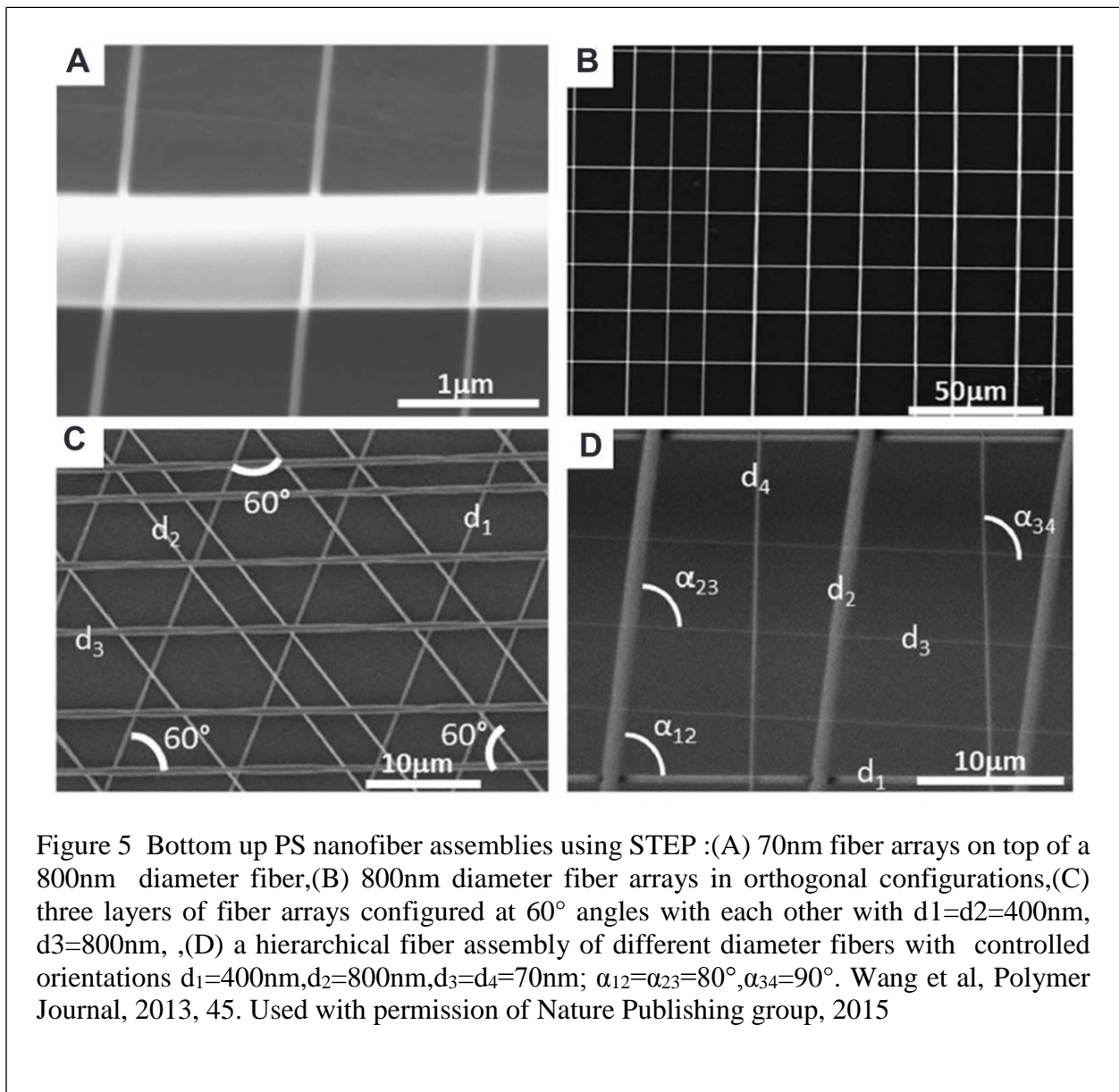
Manipulating nanofibers into patterns/assemblies is of great interest because of their potential application in sensors, bio-implantations and smart textiles. Intensive efforts have been devoted to achieve nanofiber assemblies and patterns using electrospinning, direct drawing and rotary jet-spinning. Using these approaches, nanofiber assemblies in forms of unidirectional arrays, cross-bars and stacked membranes were achieved. However, the uniformity of constituent nanofiber dimensions and inter-fiber spacing is difficult to control. In contrast to these approaches, STEP is



capable of obtaining nanofiber assemblies with unique control of fiber dimensions, spacing and orientations. Uniform diameter STEP fibers are configured in parallel arrays as they are collected on substrates and the space between fibers is easily controlled by adjusting the substrate translation speed. At constant rotating speed, fiber spacing is directly proportional to the translation speed. Additionally, layers of fiber arrays can be deposited on top of previous layers at any desired angle. Due to absence of electric fields, sub 100 nm diameter fibers can be easily deposited in the form of evenly spaced uniform fiber arrays without being disturbed by spinning instabilities. In Figure



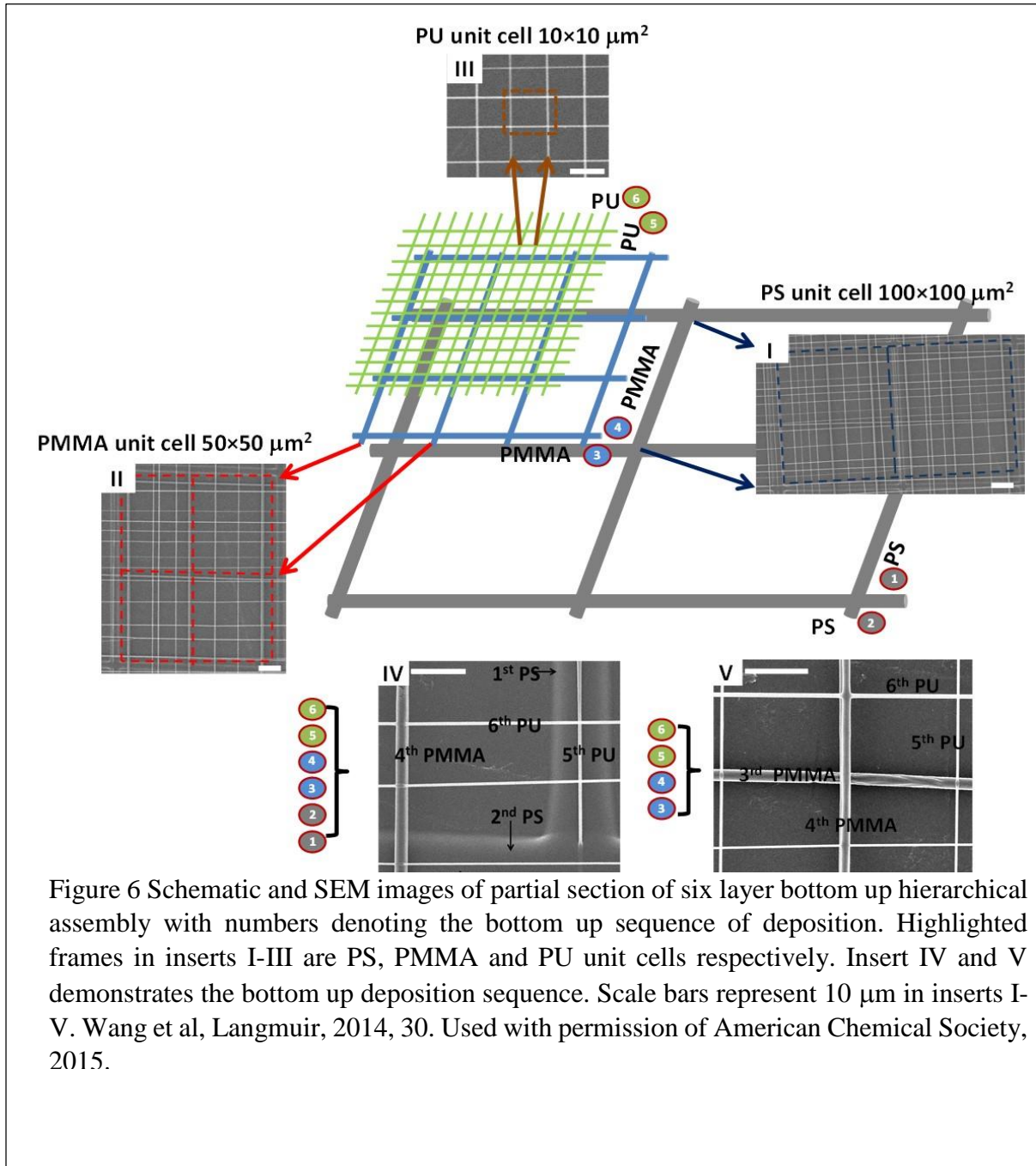
5(A) and (B), we demonstrate 70 nm diameter fiber arrays on top of a 800nm diameter fiber and a crisscross fiber assembly of 800 nm diameter fibers (forming a matrix of rectangular unit cells). [51] Notice that from Figure 5(A) to (B), the fiber spacing was increased from 1  $\mu\text{m}$  to 16  $\mu\text{m}$  by increasing translation speed from 0.02 mm/s to 0.32 mm/s. More complex fiber patterns were achieved by stacking several layers of fiber arrays together while varying the inter-layer angles. Figure 5(C) demonstrates an assembly of three layers of fiber arrays (diameters:  $d_1=d_2=400$  nm,  $d_3=800$  nm) deposited at  $60^\circ$  angles to each other, creating equilateral triangles. In addition, large



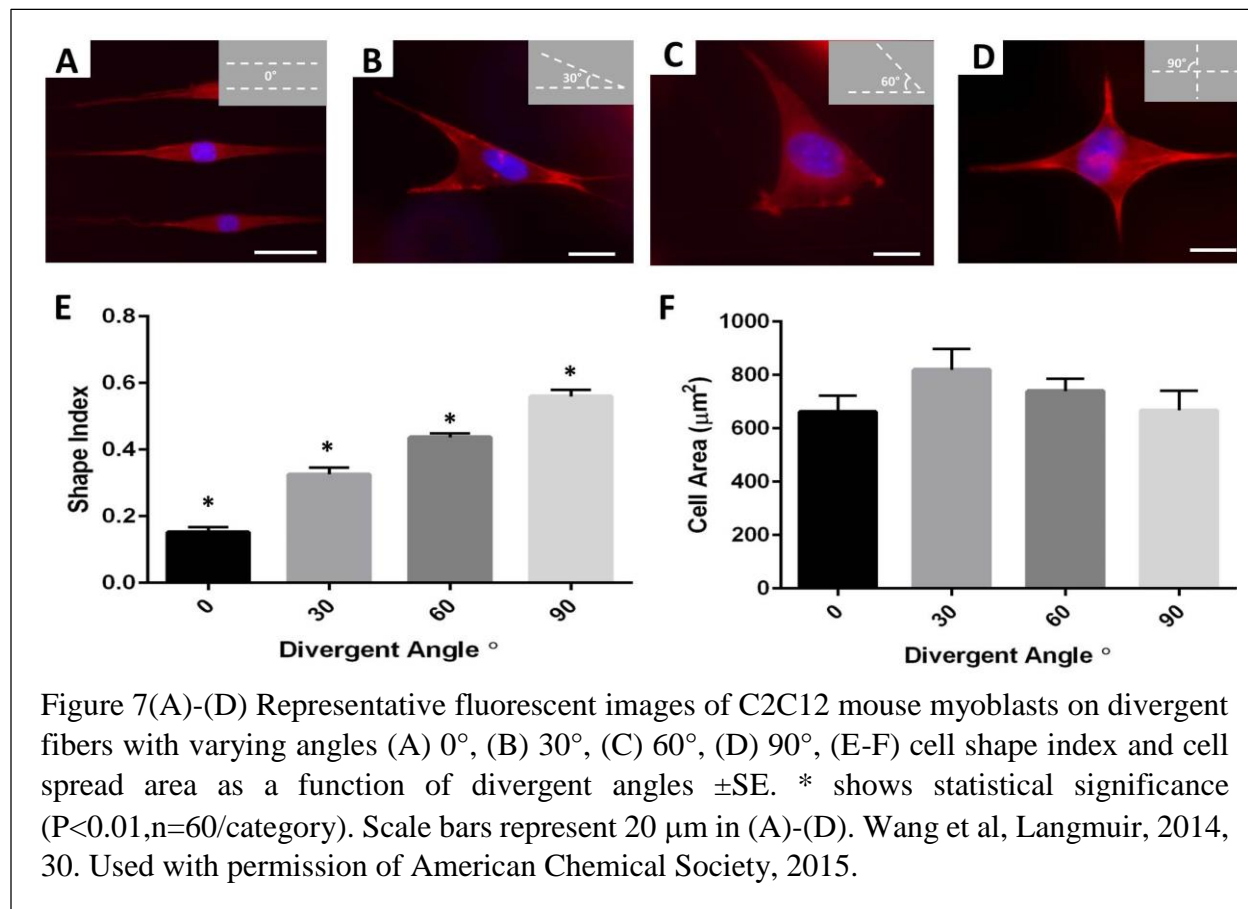
diameter fiber networks can be used as basis of the assembly, over which sub 100 nm diameter fiber networks form the top structures, thus creating a bottom up hierarchical structure. Figure 5(D) demonstrates such a hierarchical assembly, which incorporates base layers made of medium diameter fibers ( $d_1=400$  nm) and large diameter fibers ( $d_2=800$  nm) and top structure made of small diameter fibers ( $d_3=d_4=70$  nm) with controlled orientations ( $\alpha_{12}$ ,  $\alpha_{23}$ ,  $\alpha_{34}$ ) and fiber spacing.

As shown in Figure 6, using STEP fibers as 1D building blocks, we then developed a suspended 6 layer scaffold (thickness  $\sim 12$   $\mu\text{m}$ ) in which large diameter PS fibers (diameter  $\sim 5$   $\mu\text{m}$ ) were first deposited in two layers at unit cell area of  $100 \times 100 \mu\text{m}^2$ . [46] The third and fourth layers of PMMA fiber (diameter  $\sim 1$   $\mu\text{m}$ ) were deposited at  $50 \times 50 \mu\text{m}^2$  unit cell size on top of PS fibers and finally, fifth and sixth layer of PU fibers (300 nm in diameter) were deposited on top of PMMA fibers at  $10 \times 10 \mu\text{m}^2$  unit cell size. To maintain fiber conformations (fiber spacing and orientation), each new layer was fused to the previously deposited layers at the intersections using an in-house solvent vapor treatment method. Using STEP, there is potentially no limitation on the numbers of layers that can be stacked on top of each other and the architectures of each layer (fiber material, diameter and conformation) can be customized as required.

A large number of studies using flat or gel culture systems have highlighted the role of extrinsic biophysical cues from the surrounding extra-cellular matrix (ECM) on cellular interactions.[52,53] Topographic reactions of cells to micro-meter range features such as wells, islands, and pillars have been intensively investigated based on micro-patterned approaches.[54] It has been shown that cell shape, position and function can be regulated by attachment of cells on engineered



substrates coated with different density of ECM.[55,56] However, cells require a full description of 3D nanofibrous ECM to maintain their phenotypic shape and establish behaviour patterns. Recently, electrospun nanofibrous scaffolds have been successfully produced from both synthetic and natural polymers with diameter ranging from nanometer to micrometers.[34,57] Cell studies on these scaffolds have revealed that cell attachment and spreading is affected by nanofiber diameter and scaffolds porosity.[58,59] However, the role of suspended fiber spacing and orientation in influencing cell behavior has yet to be demonstrated. Cells on suspended fibers react to mechanical cues by wrapping around the suspended fibers, which has been shown by us to elicit different cell behaviors.[8,33,60–62] Suspended cell-fiber culture systems afford a wide parametric investigation of the role of topographical cues on cellular interactions. In this study, we present the development of hierarchical nanofiber assemblies as a platform technology to control

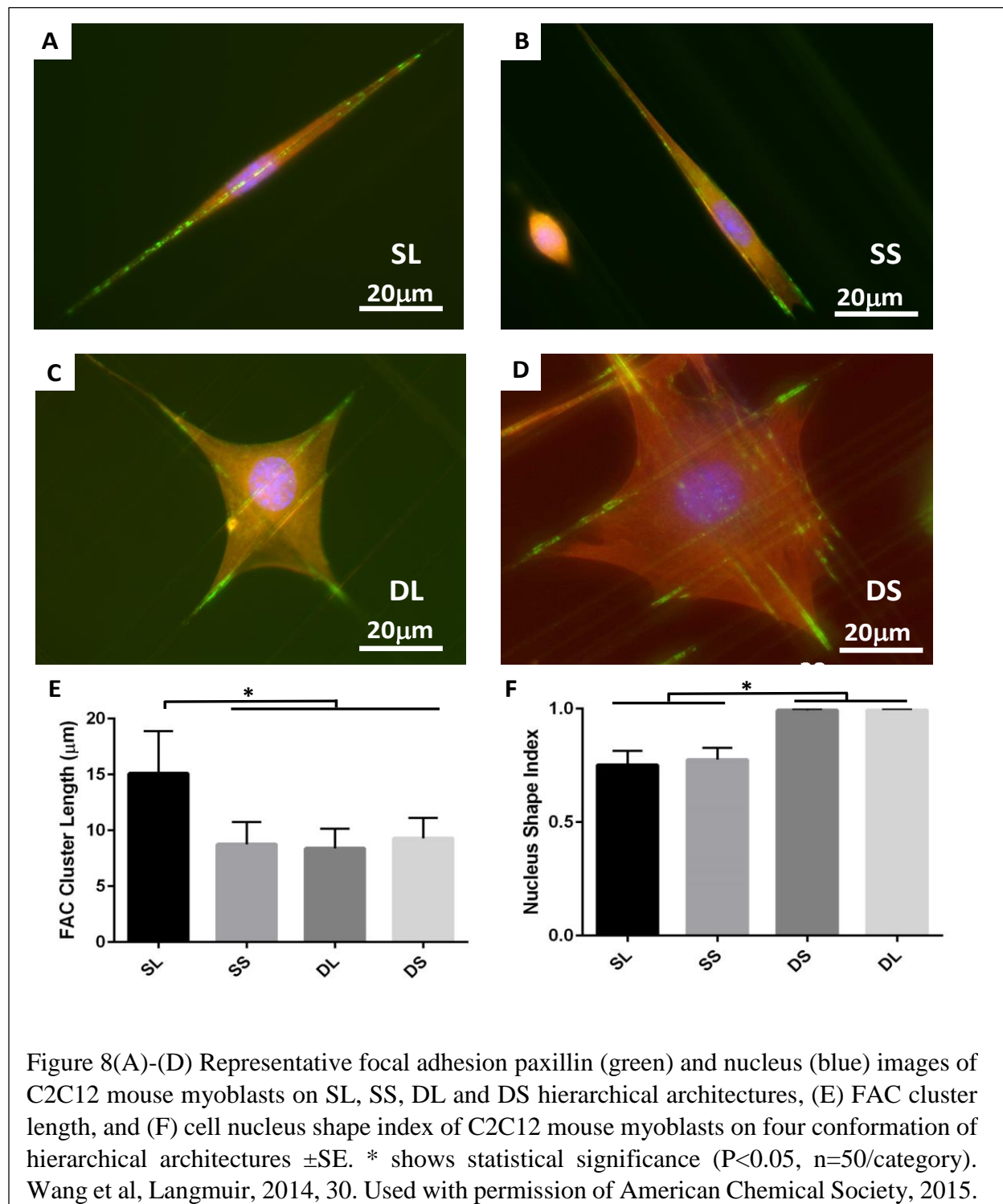


cell geometry with the aim of studying the arrangement of cellular cytoskeleton on suspended fiber networks.

Geometric shapes of cells are known to play an important role in directing DNA synthesis, cell growth and apoptosis.[63,64] To control cell geometric shapes, suspended nanofibers with varied divergent angles were prepared. As shown in Figure 7 (A-D), C2C12 mouse myoblasts seeded on suspended PS nanofibers (diameter~300nm) with divergent angles ( $0^\circ$  to  $30^\circ$ ,  $60^\circ$  and  $90^\circ$ ), attached and formed shapes that closely matched the shape of the underlying divergent nanofibers. [46]The simplest spindle shape was formed on parallel fibers ( $0^\circ$ ), and with increase in the divergent angle, cells spread on multiple fibers, forming polygonal shapes. Correspondingly, cell shape index  $SI$  ( $SI = \frac{4\pi A}{p^2}$ , where  $A$  is the cell area and  $p$  is the cell perimeter) demonstrated pronounced increase (from 0.15 to 0.57) with increasing divergent angles (Figure 7 (E)). Interestingly, as the cell shape varied on divergent nanofibers, the cell area was maintained relatively constant (Figure 7 (F)). To the best of our knowledge, this is the first time that cell shapes are precisely controlled through the divergent angles between suspended nanofibers.

Focal adhesion sizes have long been reported to play a critical role in cell migration, with larger focal adhesion size on flat substrates indicating decreased migration speed.[65,66] In our study, cells on nanofiber assemblies are forced to form focal adhesion clusters at the cell periphery and along the fiber axis, as shown in Figure 8(A-D). [46]Our results demonstrate that cells form significantly longer focal adhesion complex (FAC) clusters ( $\sim 15\mu\text{m}$ ) on SL (single layer with large spacing) assemblies (Figure 8(E)), which are consistent with our previous findings.[33] The results indicate that it is possible to control focal adhesion size through manipulating conformations of

nanofiber assemblies. Furthermore, the FAC cluster lengths are more than 8  $\mu\text{m}$  on all four conformations SL (sing layer with large fiber spacing 20  $\mu\text{m}$ ), SS ( single layer with small fiber spacing 5  $\mu\text{m}$ ), DL (double layer with large spacing 20  $\mu\text{m}$ ) and DS (double layer with small



spacing 5  $\mu\text{m}$ ) , which are significantly longer than previous reported FAC lengths on flat substrates (1-6  $\mu\text{m}$ ).[67,68]

Cellular geometry can elicit different nucleus shapes due to coupling of nucleus with the cytoskeleton.[69,70] Nucleus shape deformation has been proposed to cause conformational changes in chromatin structure and organization and directly affect gene expression and protein synthesis.[71,72] On suspended fibers, as shown in Figure 8 (F), the nuclei became elongated (nucleus shape index  $SI \sim 0.75$ ) as the cell formed spindle shapes on unidirectional nanofiber assemblies (SL and SS), while on crisscross nanofiber assemblies (DL and DS), the nuclei appeared rounded (nucleus shape index  $SI \sim 0.99$ ) within the polygonal-shaped cells. Our results indicate that cell nucleus shape can be modulated by topographical cues of the nanofiber assemblies, thus influencing nuclear functions and possible cell functions.

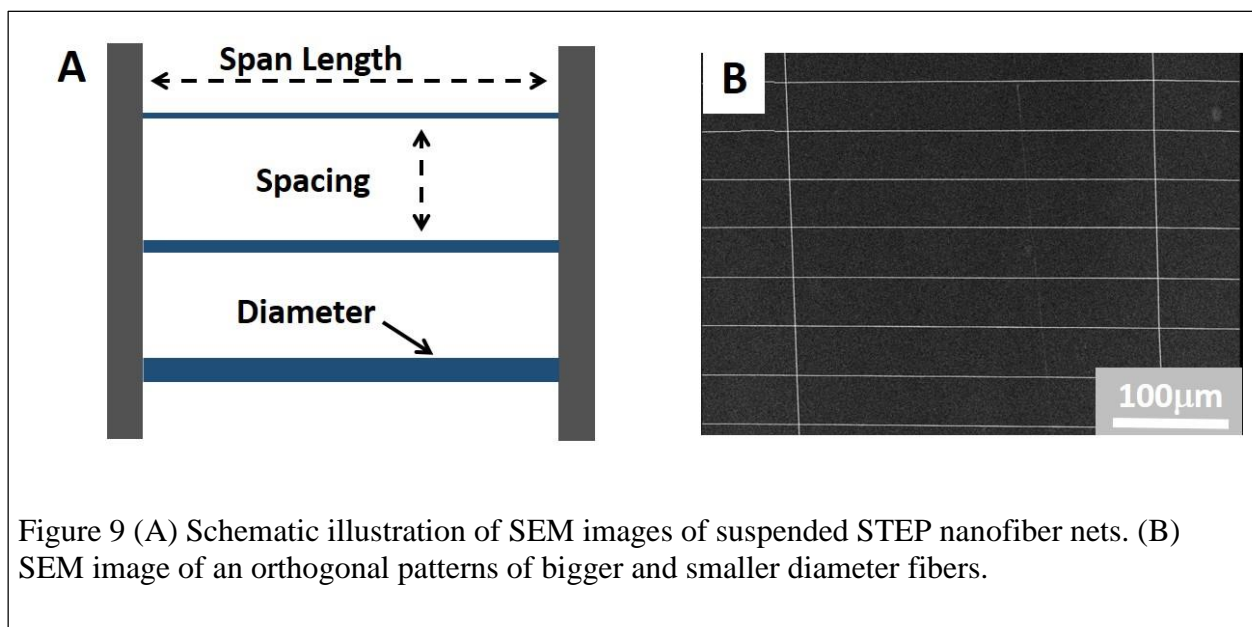
In conclusion, suspended nanofiber scaffolds with precisely controlled fiber orientation have been developed using the STEP technique, which offers an opportunity to closely represent the native environments aimed at recapitulating cell behaviors *in vitro*. The suspended nanofibers cause cells to react to surface curvature and dimensionality that flat substrates inherently mask, thus enabling a unique platform for investigating cell-fiber interactions as measured by a number of metrics such as cell geometries, densities, spread areas, cluster length and cell nucleus shapes. The suspended nanofiber assemblies provide cells with simultaneous 1, 2 and 3D cues, as cells are able to align along the fiber axis (1D), spread between multiple fibers (2D) and wrap around fibers (3D). Our results suggest that exquisite topographical cues from the nanofiber assembly can potentially control cell behaviors and functions. We envision that exquisitely deposited suspended nanofibers

on varied three dimensional shapes could find wide applications in diverse fields such as wound healing, organ regeneration and developmental and disease biology.

### 3.3 Contractile Cell Force Probes using Suspended Nanofiber Networks

#### 3.3.1 Fabrication and Characterization of Nanofiber Nets

Stem cells possess a unique ability to differentiate into a number of committed lineages in response



to physical cues. Physical interactions with ECM induce cell forces, which influence critical cell behaviors such as attachment, spreading, migration, and cell differentiation. Forces exerted by single cells can range from pico Newtons to micro Newtons, which are measured by a variety of existing platforms such as micropillar arrays and deformable flat gels. In the latter case, displacements of beads embedded randomly throughout the gel are correlated to deformation generated by cells. However, the relation between bead displacements and force is difficult to compute. [73,74] An alternative strategy has been to use micro-dimensional force sensor arrays



( $\mu$ FSA) such as micropillars/posts. The deflection of the pillar/post caused by the attached cell is a direct measurement of the local forces. [75,76] However, fabrication of the micropillars with precisely controlled dimensions (cross-sections, height and density) is challenging and tracking the deformation of posts can be time consuming. So far, both approaches have provided important quantitative information on force distributions and has led to significant improvement in understanding of spatial and temporal traction response of cells. However, these platforms are unable to capture the physical features of *in-vivo* fibrous ECM, namely fiber diameter and fiber bending stiffness (N/m). Based on the hierarchical nanofiber assemblies, we developed nanofiber nets, which topographically and mechanically mimic the fibrous ECM and offer an approach to measure cell forces conveniently.

Most of the cells do not only apply forces but also respond through cytoskeleton organization to the resistance that they sense with regard to the stiffness of the matrix. Here, the nanofiber nets are developed to quantify the effects of fiber stiffness on mesenchymal stem cell (MSC) forces. As shown in Figure 9, nanofiber nets are achieved by fusing nanofibers with microfibers at the intersections. The diameter, suspended length and spacing of nanofibers can be precisely controlled using the STEP technique. Using the STEP technique, suspended and aligned micron fibers (diameter 2-3  $\mu\text{m}$ ) and nanofibers (diameter 200-1000 nm) were deposited in orthogonal patterns and fused at the intersections using a custom solvent evaporation device. The nanofibers were deposited precisely to control the suspended length from 50 to 300  $\mu\text{m}$  to observe measurable fiber deflection.

The deflection of the suspended nanofibers is a direct measurement of the contractile cell forces. To calculate cell contractile forces, mechanical properties (stiffness and modulus) of single suspended nanofibers are characterized through an AFM based three point bending test. By deflecting a single suspended nanofiber at the middle, a force-deflection curve can be achieved, the slope of which gives the apparent stiffness value  $k_{app}$  of the nanofiber, as shown in Figure 10. As proposed by Caenot *et al.*, the apparent stiffness value of a nanofiber/nanowire can be expressed as [77]:

$$k_{app} = k + k_T = \frac{192EI}{L^3} + \frac{24T}{5L}$$

Equation 1

Where  $k$  and  $k_T$  are contributions of structure stiffness and tension in the fiber respectively. In our study, we assume the tensile stress is uniformly distributed across the cross-section of the fiber, and therefore we can re-write Eq 1 as:

$$k_{app} = k + k_T = \frac{192EI}{L^3} + \frac{6\pi\sigma_R D^2}{5L}$$

Equation 2

Where  $D$  is the fiber diameter and  $\sigma_R$  is the tensile stress built during the manufacturing process.

Multiplying both sides of Eq 2 with  $L/D^2$ , we have :

$$k_{app} L/D^2 = 3\pi E \left(\frac{D}{L}\right)^2 + \frac{6\pi\sigma_R}{5}$$

Equation 3

Reporting apparent modulus multiplied by  $L/D^2$  versus geometrical parameter  $\left(\frac{D}{L}\right)^2$  should give a linear relation, as shown in Figure 11. The linear regression allows the determination of elastic modulus  $E$  and tensile stress  $\sigma_R$  (summarized in Table 3), as the slope is proportional to the elastic

modulus  $E$  and the non-zero intercept is proportional to the tensile stress  $\sigma_R$ . Note that the determined elastic modulus of PS nanofiber is 0.97 GPa, which is comparable to the bulk material.

The cells were assumed to exert contractile loads through focal adhesions, which are located at both edges of the cell, as is indicated by stained paxillin images (Figure 8).

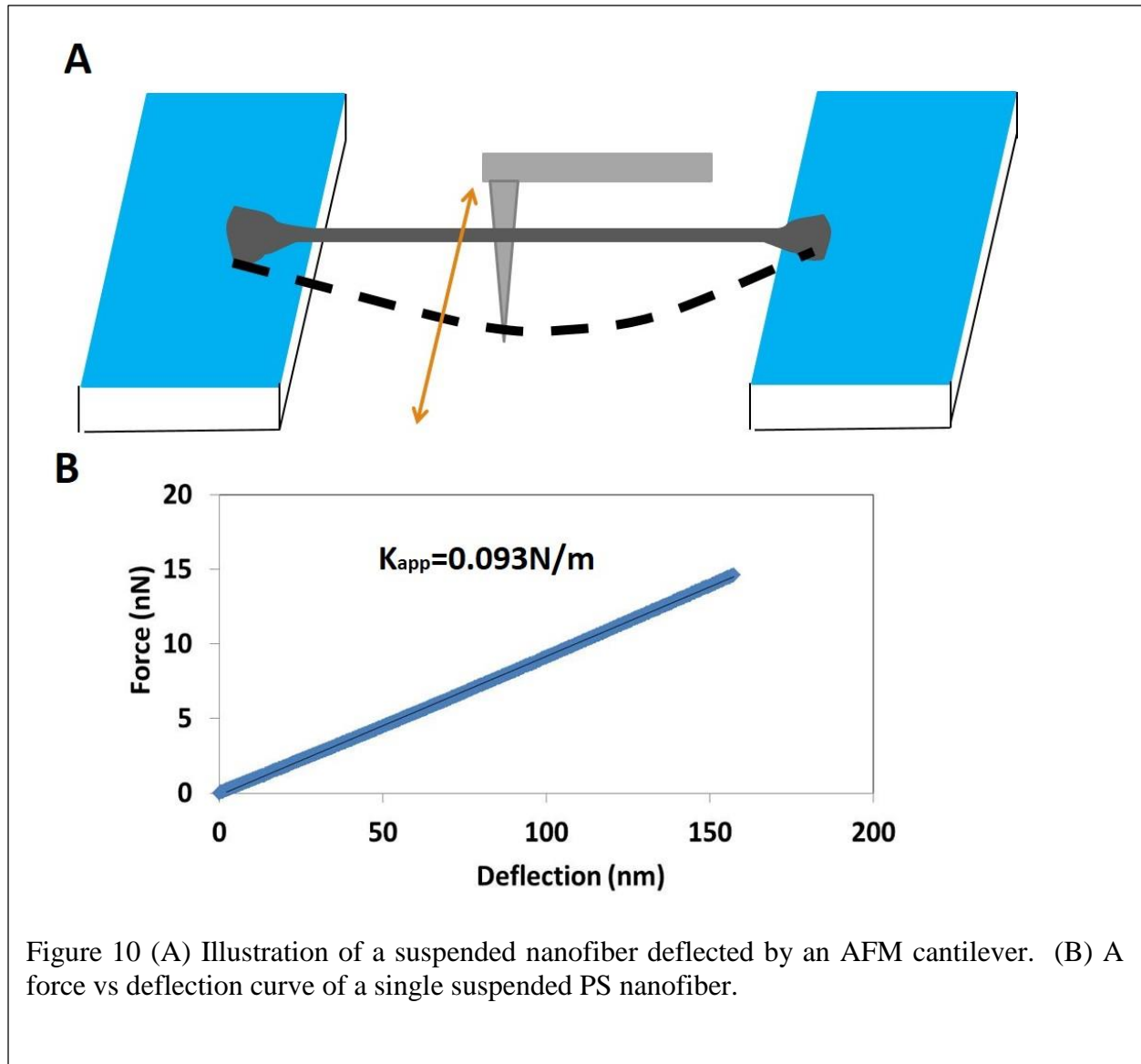


Figure 10 (A) Illustration of a suspended nanofiber deflected by an AFM cantilever. (B) A force vs deflection curve of a single suspended PS nanofiber.

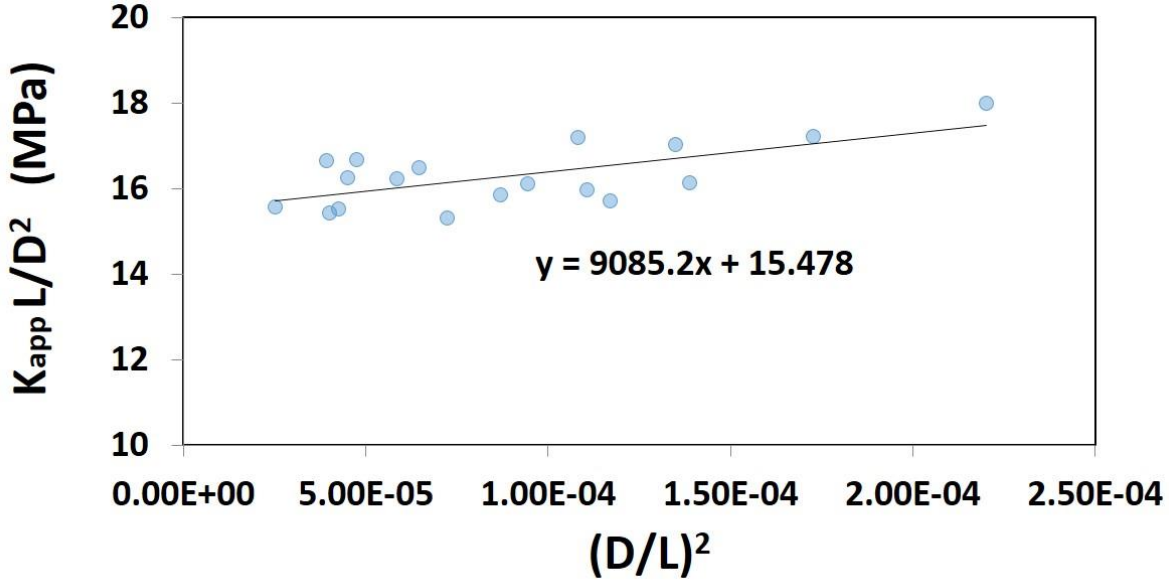


Figure 11 Product of apparent stiffness  $k_{app}$  and  $L/D^2$  of PS nanofibers as a function of  $(D/L)^2$

Table 3 Mechanical Properties of single PS nanofibers

Slope (MPa)	Modulus (GPa)	Intercept (MPa)	Tensile Stress (MPa)
9085.22	0.97	15.48	4.10

For cell force calculation, we use the “tie rod” model as shown in Figure 12 (A). Suspended nanofibers were considered as prismatic beams with “pin-pinned” boundary conditions. We assume the beam is under tension with small beam deflections. Under these conditions, the cell contractile loads  $P_1$  and  $P_2$  can be obtained by solving the following equations:

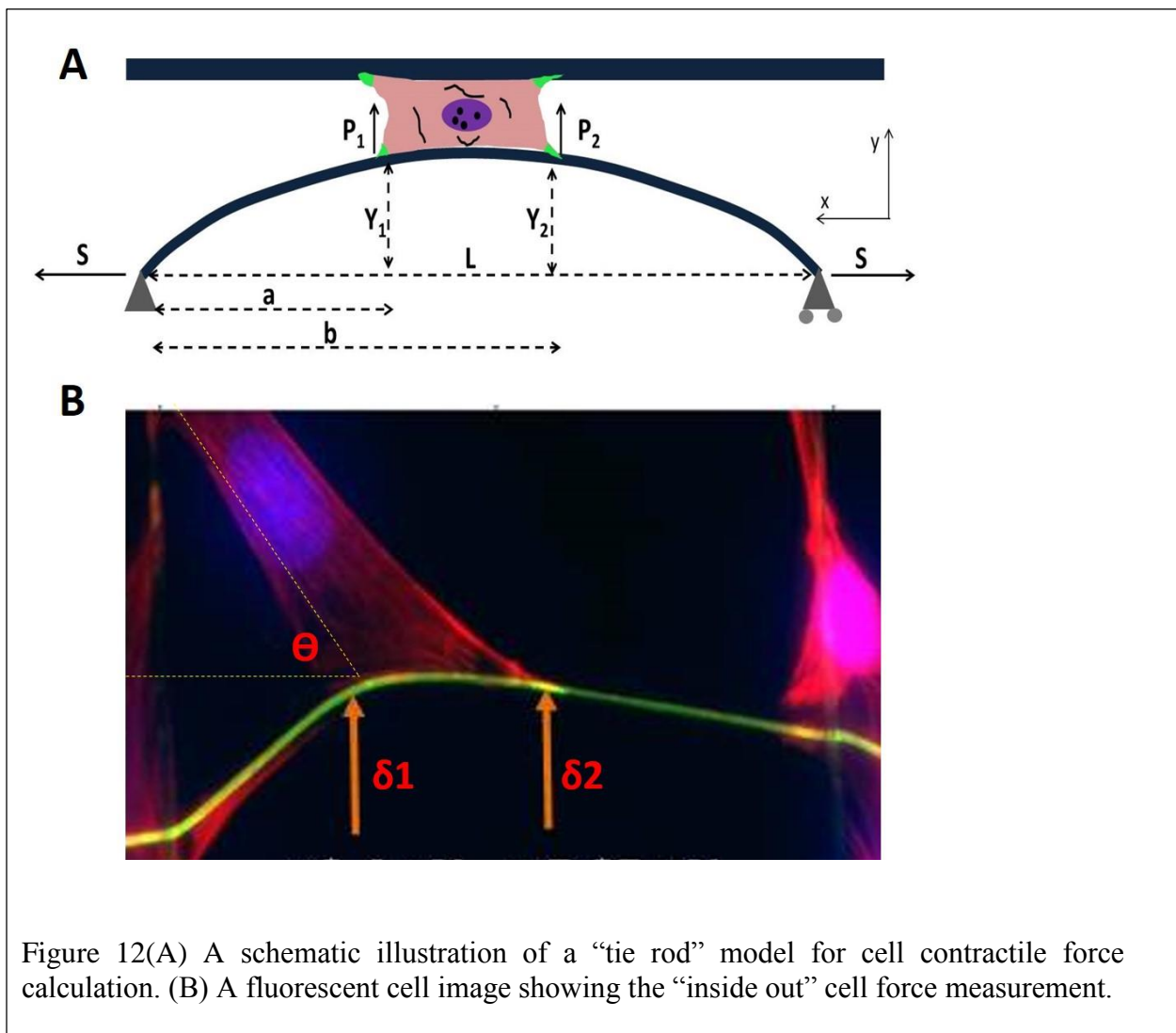
$$-\frac{P_1 \sinh[\lambda(L-a)]}{S\lambda \sinh[\lambda L]} \sinh[\lambda a] + \frac{P_1(L-a)}{SL} a - \frac{P_2 \sinh[\lambda(L-b)]}{S\lambda \sinh[\lambda L]} \sinh[\lambda a] + \frac{P_2(L-b)}{SL} a = Y_1$$

Equation 4

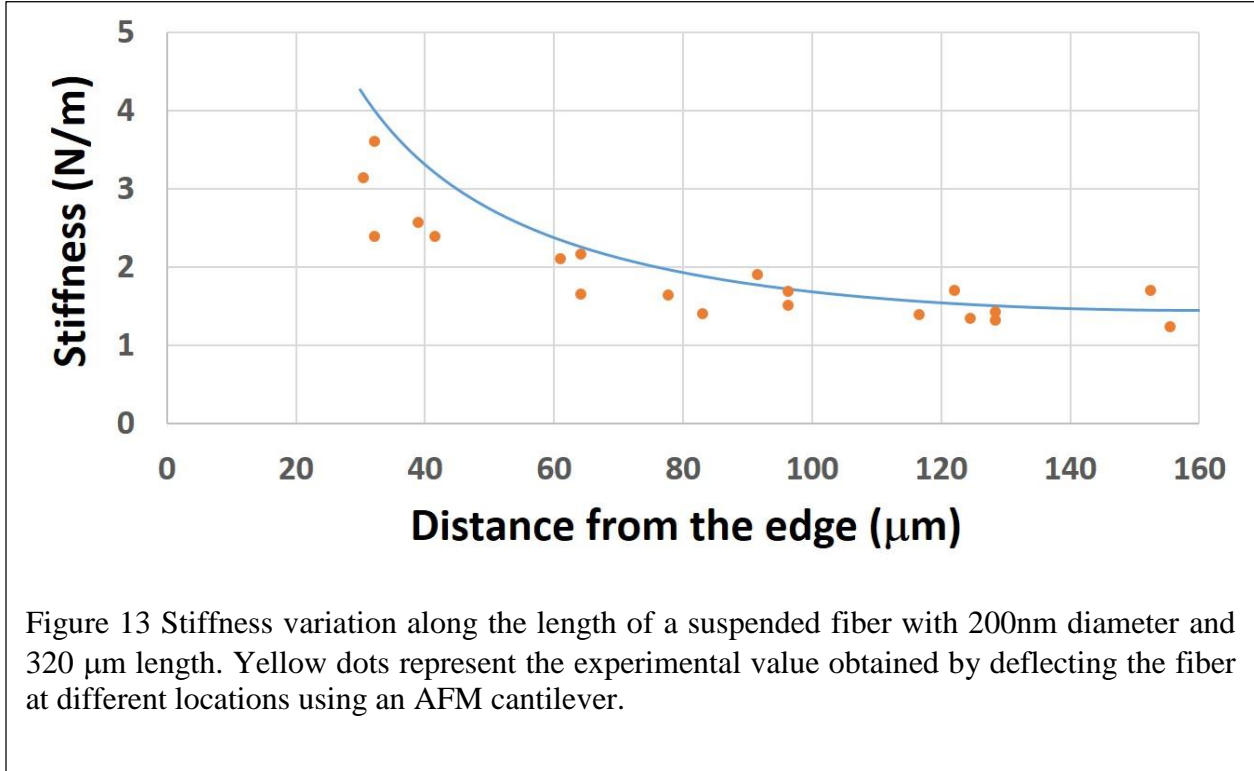
$$-\frac{P_1 \sinh[\lambda a]}{S\lambda \sinh[\lambda L]} \sinh[\lambda(L-b)] + \frac{P_1(L-b)}{SL} a - \frac{P_2 \sinh[\lambda(L-b)]}{S\lambda \sinh[\lambda L]} \sinh[\lambda b] + \frac{P_2(L-b)}{SL} b = Y_2$$

Equation 5

Where  $\lambda = \sqrt{\frac{S}{EI}}$ , E, I and S are fiber modulus and second moment of inertia and tensile load respectively.  $Y_1$  and  $Y_2$  are beam deflections at locations a and b, L is the length of the beam.



As mesenchymal stem cell stretched along the STEP nanonets, the smaller diameter fibers were deflected. (Figure 12 (B)). The deflection at both ends of the cell and the respective angle of deflection “ $\Theta$ ” (line drawing along the cell body, signifying high concentration of of F-actin stress fibers) were measured.



The stiffness along a suspended fiber length was calculated from Eq 6:

$$k = \frac{P}{y} = \frac{1}{\frac{-\sinh[\lambda a]}{S\lambda \sinh[\lambda L]} \sinh[\lambda(L-x)] + \frac{a}{SL}(L-x)}$$

Equation 6

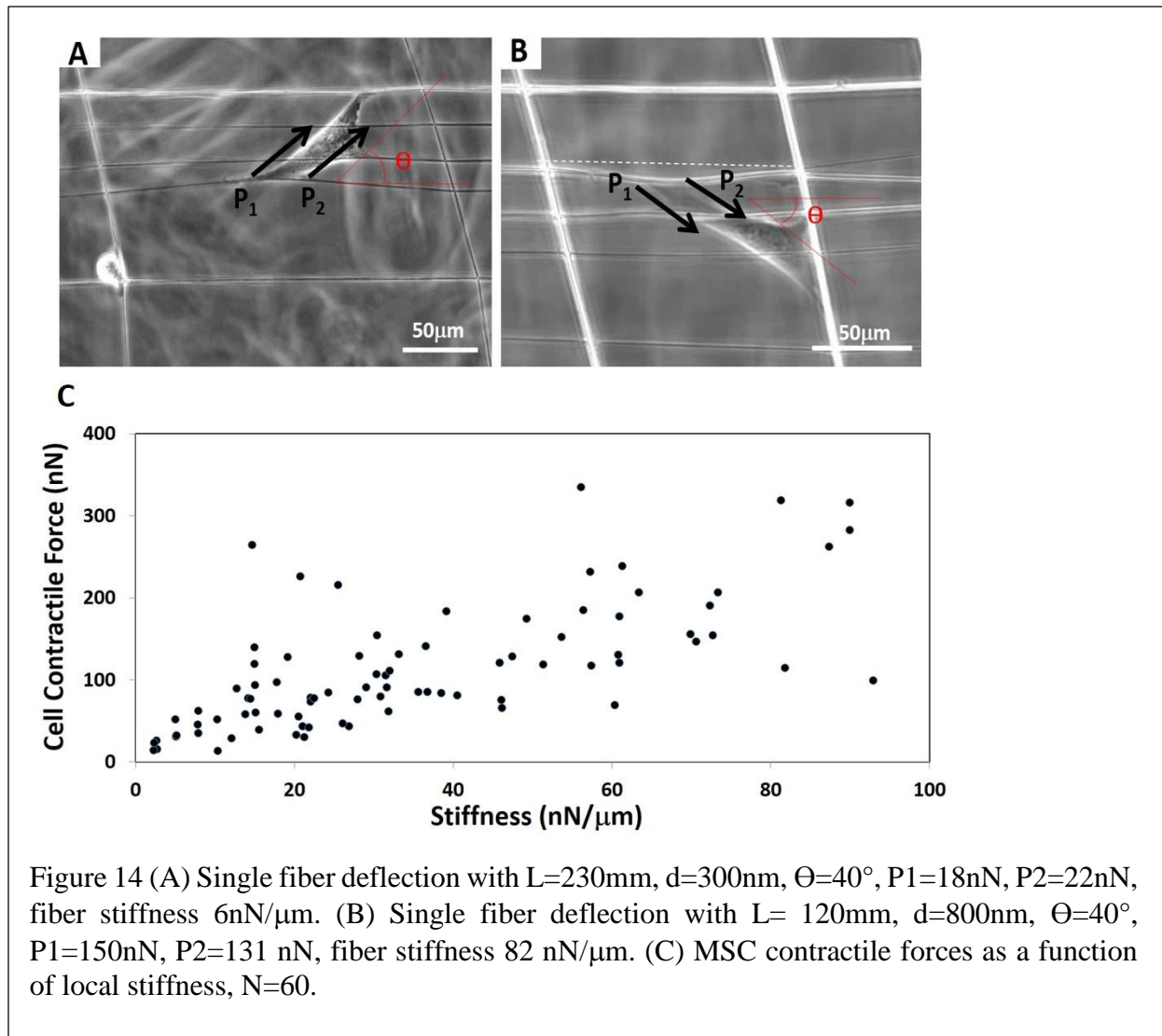
The calculated results were verified by deflecting a suspended nanofiber at different locations using an AFM cantilever, as shown in Figure 13. With known mechanical properties of the polystyrene nanofibers (Young’s modulus ~0.97 GPa, stress built in the fiber ~ 4.1 MPa), the fiber stiffness can be varied through adjusting diameter and suspended length. In our current study, the

fiber stiffness is varied from 1 nN/ $\mu\text{m}$  (corresponding to dia~150 nm, length~300  $\mu\text{m}$ ) to 300 nN/ $\mu\text{m}$  (corresponding to dia~1000 nm, length~50  $\mu\text{m}$ ). The stiffness range we used in this study has covered the full range achieved by poly(dimethylsiloxane) (PDMS) micropillar arrays. Although the stiffness of the micropillars can be manipulated by changing the diameter and length, there is a lower limit of stiffness (~10 nN/ $\mu\text{m}$ ) achieved in this way due to the limitation of the pillar length.[74] In contrast, nanofiber nets offer us a straightforward approach to adjust the stiffness within a wide range of three orders of magnitude by controlling the fiber dimensions (diameter and suspended length). Note that it is convenient for us to achieve nanofibers with stiffness less than 1nN/ $\mu\text{m}$  by increasing the fiber length.

### **3.3.2 Mesenchymal Stem Cell Contractile Force Measurement based on Nanofiber Nets**

In our experiment, we observe MSCs contractile force ranging from 18 nN to 350 nN, depending on the stiffness of the fiber. (Figure 14) Large diameter fiber with short suspended length leads to larger contractile forces. In our study, cell forces increases with stiffness in the range of 2 nN-100 nN. The increase of cell force with stiffness suggests that the matrix strain may be sensed by cells as tactile set point—cell contraction forces are regulated to achieve a certain deformation of the matrix, which is supported by previous studies of Discher et al. [78]

Using STEP nanonets, the biophysical interactions of single MSC cells with suspended fibers provide us with new insights into cell mobility, which can be coupled with a force response and stiffness variation. In particular, the platform provides the ability to measure the forces exerted by single MSC cells as they migrate along nanofibers.





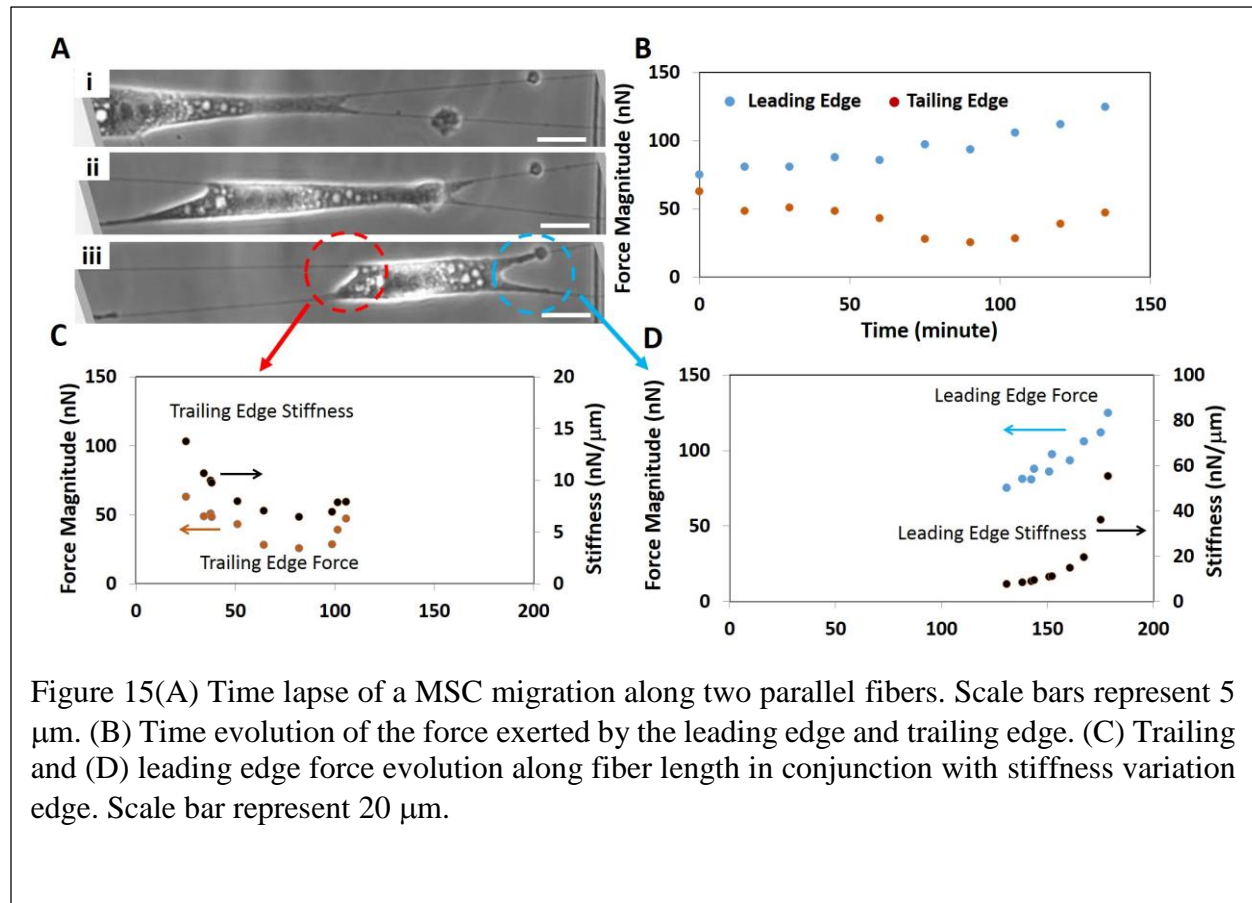
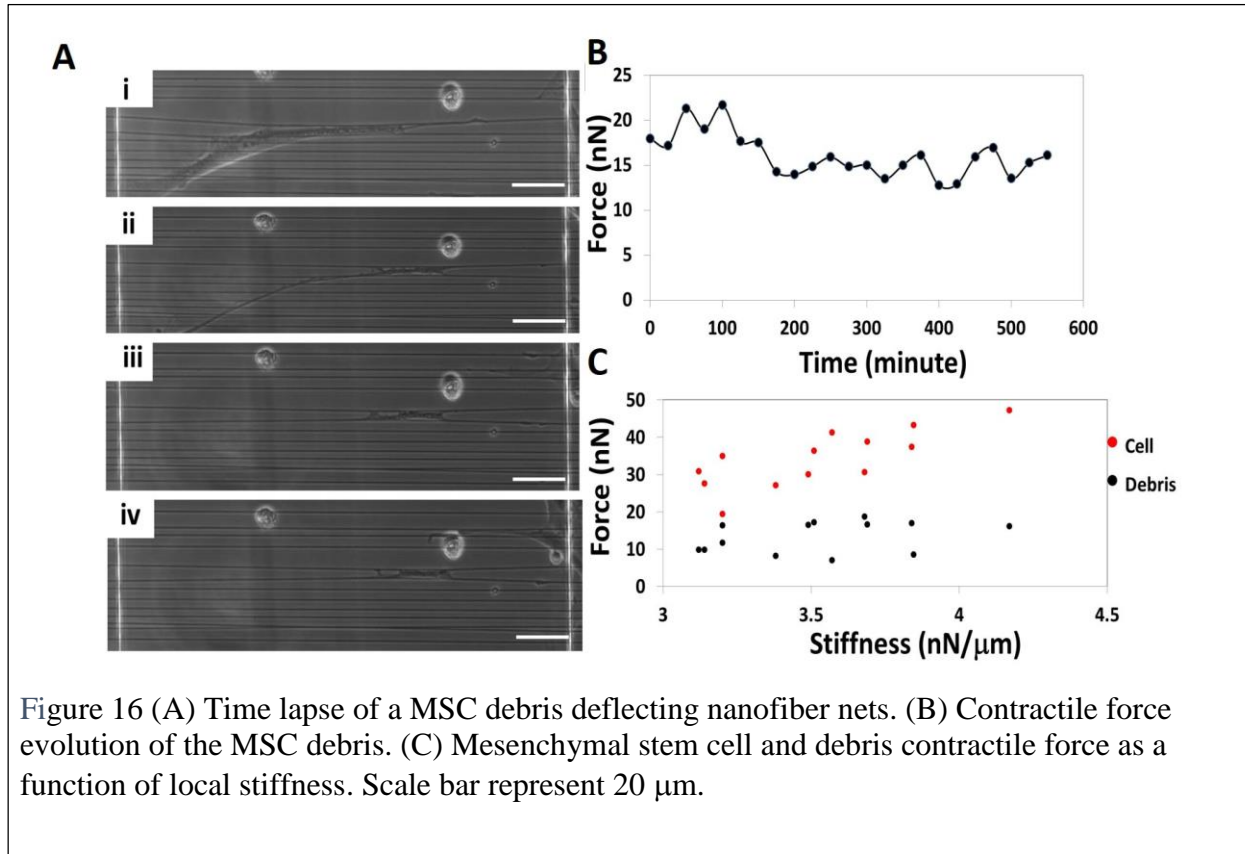


Figure 15(A) Time lapse of a MSC migration along two parallel fibers. Scale bars represent 5  $\mu\text{m}$ . (B) Time evolution of the force exerted by the leading edge and trailing edge. (C) Trailing and (D) leading edge force evolution along fiber length in conjunction with stiffness variation edge. Scale bar represent 20  $\mu\text{m}$ .

As shown in Figure 15, MSCs adhered to parallel fibers exert higher forces at the leading edge compared to the trailing edge. Furthermore, the evolution of contractile forces exerted by leading and trailing edges scale with structural stiffness.

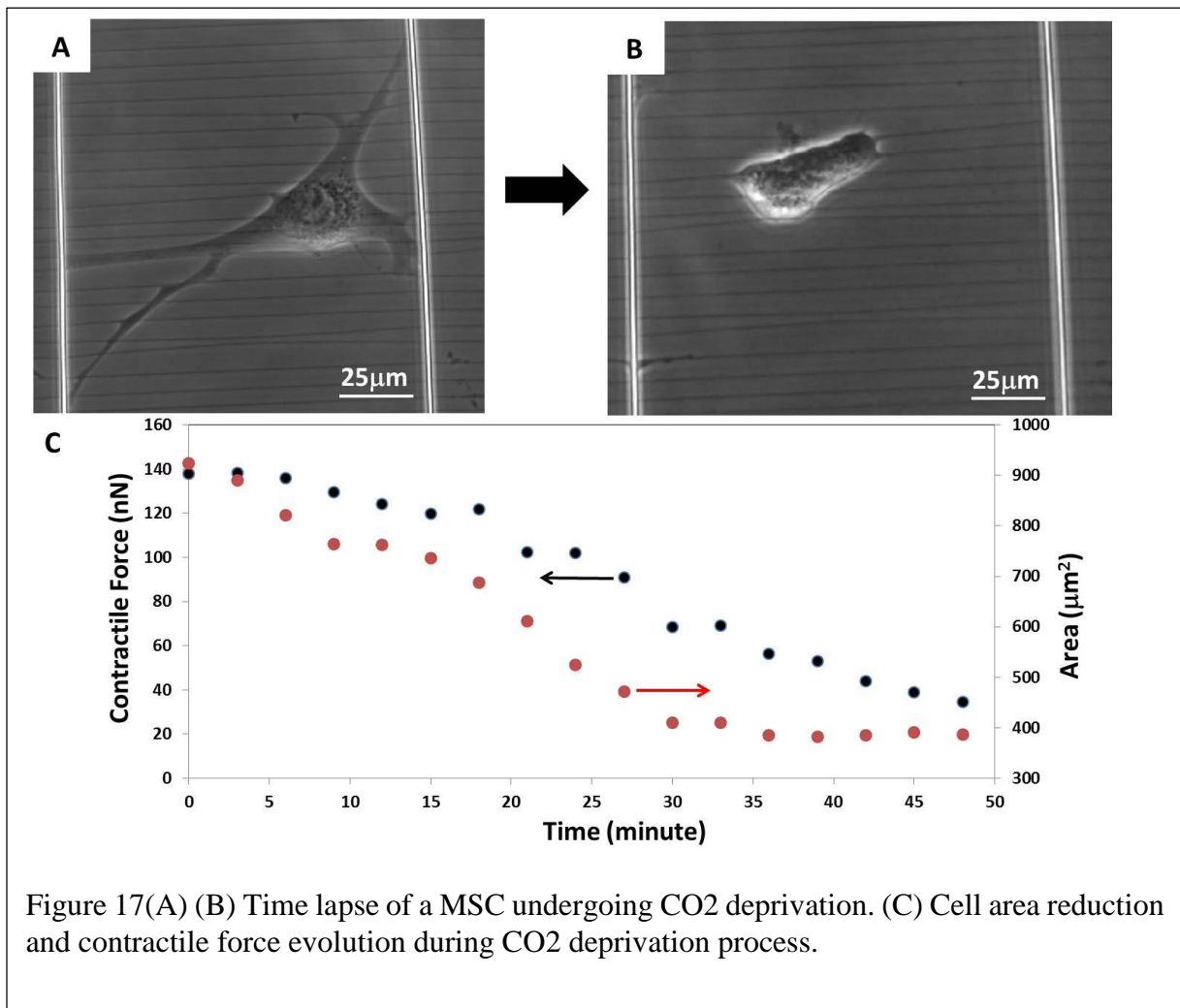
In our experiment, cells were observed to shed debris (Figure 16 (A)) and the contractile forces of debris was recorded as shown in Figure 16 (B). It is interesting to note that MSC debris continuously exerts contraction (15-20 nN) for about 10 hours. Compared to MSC cell body forces, debris forces are lower and do not respond to the stiffness variation in the stiffness range 3 nN/ $\mu\text{m}$ -4.5 nN/ $\mu\text{m}$ . (Figure 16 (C)).

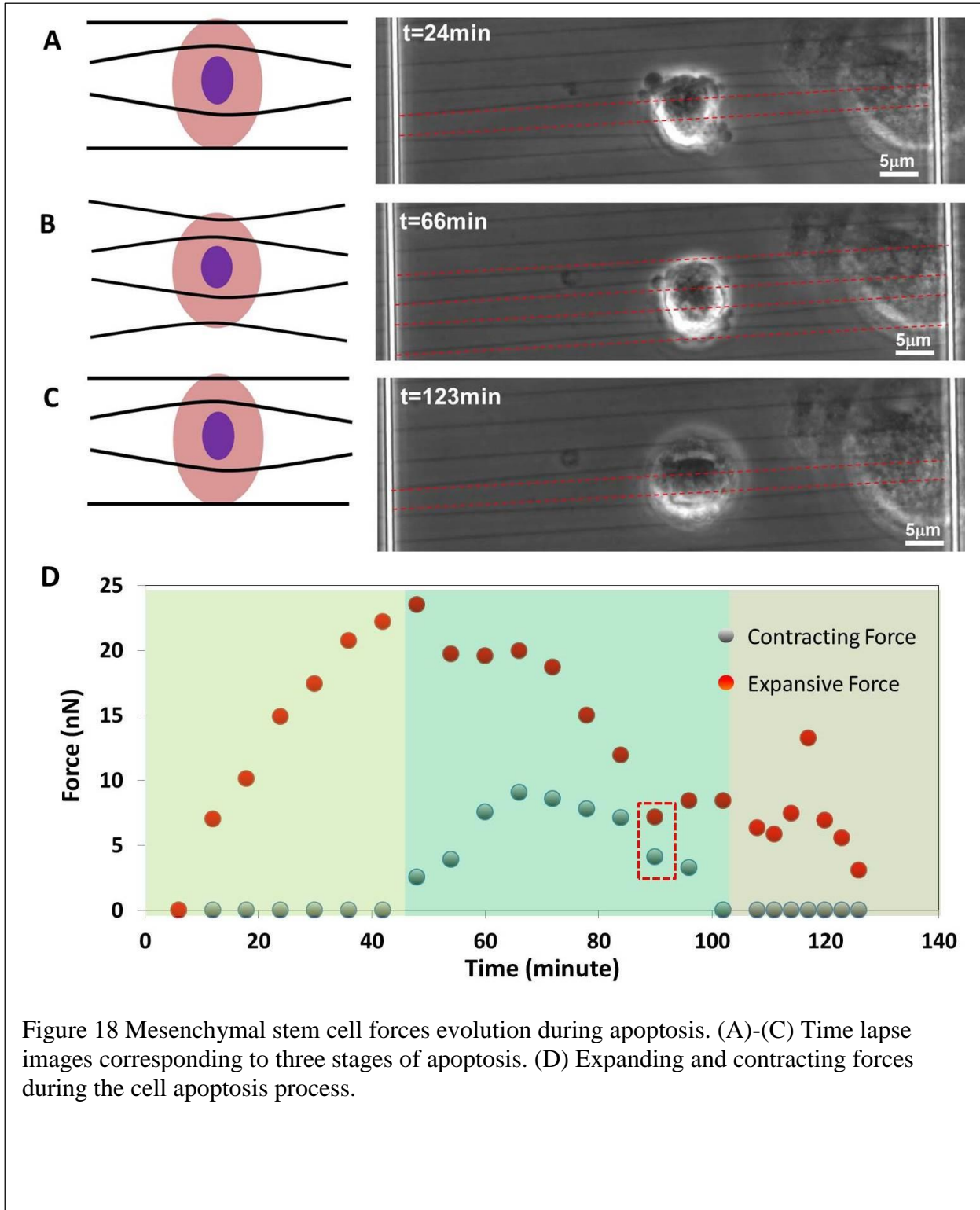


MSCs respond to  $\text{CO}_2$  deprivation by monotonic area reduction and contraction force decrease, which leads to a reduced cell shape and cell apoptosis, as shown in Figure 17.

MSCs are observed to exert both contractive and expansive forces simultaneously during apoptosis process (Figure 18), which signifies the role of actomyosin based cortex contractility in MSCs apoptosis process. [55,79] It is interesting to note that contractive and expansive forces reached comparable magnitudes ( $\sim 7$  nN,  $N=21$ ) before the cell finally perishes, which may indicate an internal force balance within the apoptotic MSCs.

In this study, we developed suspended nanofiber networks to probe mesenchymal stem cell forces. Fibers possessing diameters closely resembling those of the native fibrous ECM proteins provide a curved surface for cell attachment and have structural stiffness (N/m) that can be tuned to investigate biophysical influence on cell behaviors. MSC contractile forces were found in the range of 18-320 nN, which scale with fiber stiffness. Cell debris is able to exert forces of the magnitude 15-20 nN. Cell migration forces evolution is dictated by the stiffness gradient. During apoptosis process, MSCs reduce cell spread area and exert both expansive and contractile forces. This work provides design principles for tissue engineering efforts involving tissue regeneration, oncology, developmental and disease biology.





## Chapter 4 Conclusions and Future Work

STEP technique allows collection of polymeric nanofibers of uniform dimension (diameter:sub 100nm to micrometers) in highly aligned configurations (relative angles between fibers were maintained less than  $6^\circ$ ) with well controlled inter-fiber spacing( <15%) . The STEP scaffolds were used as a platform to study single cell behaviors.

For single cell arrangement, using double layer divergent ( $0^\circ$ to  $90^\circ$ ) suspended nanofiber assemblies, we show precise quantitative control on cell geometry (change in shape index from 0.15 to 0.57 at similar cell areas). Furthermore, using unidirectional or crisscross patterns of sparse and dense fiber arrays, we are able to control cell nucleus shape index (from 0.75 to 0.99) with cells nearly doubling their focal adhesion cluster length( $\sim 15\mu\text{m}$ ) on widely spaced nanofiber arrays.

Single cell contractile forces were measured using a non-invasive “inside-out” STEP-based nanofiber net platform, which topographically represent the microenvironment of cells. Mesenchymal Stem Cells (MSCs) exerted contractile forces in range of 18nN to 320 nN which scale with the fiber stiffness, while cell debris have the ability to exert 15-20nN contractile forces on their immediate ECM. MSCs respond to  $\text{CO}_2$  depletion by decreasing cell area and reducing contractile forces. MSCs are observed to exert both contractive and expansive forces simultaneously during apoptotic process.

We demonstrate that suspended and aligned nanofibers with diameters in the range of ECM proteins can cause cell to react to structural features, such as curvature, orientation and structural stiffness ( $\text{N m}^{-1}$ ), thus provides a unique platform to investigate cell-ECM interactions.

In the future, force required to differentiate MSC cells can be measured and optimal biophysical environmental conditions required to induce MSC differentiation can be identified through careful selection of fiber diameter, suspended length and material. Optimization of ECM mimicking bio-scaffolds using STEP technique may help in general to better exploit the therapeutic potentials of stem cells. In addition, a better understanding of the mechanical transduction between single cancer cells and their environment can be achieved by integrating the current platform with microfluidic device.

## References

- [1] Guilak F, Cohen DM, Estes BT, Gimble JM, Liedtke W, Chen CS. Control of stem cell fate by physical interactions with the extracellular matrix. *Cell Stem Cell* 2009;5:17–26. doi:10.1016/j.stem.2009.06.016.
- [2] Huebsch N, Arany PR, Mao AS, Shvartsman D, Ali OA, Bencherif SA, et al. Harnessing traction-mediated manipulation of the cell/matrix interface to control stem-cell fate. *Nat Mater* 2010;9:518–26. doi:10.1038/nmat2732.
- [3] Rosso F, Giordano A, Barbarisi M, Barbarisi A. From cell-ECM interactions to tissue engineering. *J Cell Physiol* 2004;199:174–80. doi:10.1002/jcp.10471.
- [4] Fernández M, Keyriläinen J, Serimaa R, Torkkeli M, Karjalainen-Lindsberg ML, Tenhunen M, et al. Small-angle x-ray scattering studies of human breast tissue samples. *Phys Med Biol* 2002;47:577–92.
- [5] Zoumi A, Yeh A, Tromberg BJ. Imaging cells and extracellular matrix in vivo by using second-harmonic generation and two-photon excited fluorescence. *Proc Natl Acad Sci U S A* 2002;99:11014–9. doi:10.1073/pnas.172368799.
- [6] Alexander DC, Hubbard PL, Hall MG, Moore E a, Ptito M, Parker GJM, et al. Orientationally invariant indices of axon diameter and density from diffusion MRI. *Neuroimage* 2010;52:1374–89. doi:10.1016/j.neuroimage.2010.05.043.
- [7] Gritsenko PG, Ilina O, Friedl P. Interstitial guidance of cancer invasion. *J Pathol* 2012;226:185–99. doi:10.1002/path.3031.
- [8] Sharma P, Sheets K, Elankumaran S, Nain AS. The mechanistic influence of aligned nanofibers on cell shape, migration and blebbing dynamics of glioma cells. *Integr Biol (Camb)* 2013;5:1036–44. doi:10.1039/c3ib40073e.
- [9] Ushiki T. Collagen fibers, reticular fibers and elastic fibers. A comprehensive understanding from a morphological viewpoint. *Arch Histol Cytol* 2002;65:109–26.
- [10] Montgomery H, Rustogi N, Hadjisavvas A, Tanaka K, Kyriacou K, Sutton CW. Proteomic profiling of breast tissue collagens and site-specific characterization of hydroxyproline residues of collagen alpha-1(I). *J Proteome Res* 2012;11:5890–902. doi:10.1021/pr300656r.
- [11] Conklin MW, Eickhoff JC, Riching KM, Pehlke CA, Eliceiri KW, Provenzano PP, et al. Aligned collagen is a prognostic signature for survival in human breast carcinoma. *Am J Pathol* 2011;178:1221–32. doi:10.1016/j.ajpath.2010.11.076.
- [12] Friedl P, Wolf K. Plasticity of cell migration: a multiscale tuning model. *J Cell Biol* 2010;188:11–9.
- [13] Petrie RJ, Doyle AD, Yamada KM. Random versus directionally persistent cell migration. *Nat Rev Mol Cell Biol* 2009;10:538–49.

- [14] Friedl P, Wolf K. Proteolytic interstitial cell migration: a five-step process. *Cancer Metastasis Rev* 2009;28:129–35. doi:10.1007/s10555-008-9174-3.
- [15] Ekaputra AK, Prestwich GD, Cool SM, Hutmacher DW. Combining electrospun scaffolds with electrosprayed hydrogels leads to three-dimensional cellularization of hybrid constructs. *Biomacromolecules* 2008;9:2097–103. doi:10.1021/bm800565u.
- [16] Tibbitt MW, Anseth KS. Hydrogels as extracellular matrix mimics for 3D cell culture. *Biotechnol Bioeng* 2009;103:655–63. doi:10.1002/bit.22361.
- [17] Falconnet D, Csucs G, Grandin HM, Textor M. Surface engineering approaches to micropattern surfaces for cell-based assays. *Biomaterials* 2006;27:3044–63. doi:10.1016/j.biomaterials.2005.12.024.
- [18] Papenburg BJ, Vogelaar L, Bolhuis-Versteeg LAM, Lammertink RGH, Stamatialis D, Wessling M. One-step fabrication of porous micropatterned scaffolds to control cell behavior. *Biomaterials* 2007;28:1998–2009. doi:10.1016/j.biomaterials.2006.12.023.
- [19] Ito Y. Surface micropatterning to regulate cell functions. *Biomaterials* 1999;20:2333–42. doi:10.1016/S0142-9612(99)00162-3.
- [20] Wong JY, Leach JB, Brown XQ. Balance of chemistry, topography, and mechanics at the cell–biomaterial interface: Issues and challenges for assessing the role of substrate mechanics on cell response. *Surf Sci* 2004;570:119–33. doi:10.1016/j.susc.2004.06.186.
- [21] Gallant ND, Capadona JR, Frazier AB, Collard DM, García AJ. Micropatterned Surfaces to Engineer Focal Adhesions for Analysis of Cell Adhesion Strengthening. *Langmuir* 2002;18:5579–84. doi:10.1021/la025554p.
- [22] Graber DJ, Zieziulewicz TJ, Lawrence D a., Shain W, Turner JN. Antigen Binding Specificity of Antibodies Patterned by Microcontact Printing. *Langmuir* 2003;19:5431–4. doi:10.1021/la034199f.
- [23] Nelson CM, Raghavan S, Tan JL, Chen CS. Degradation of Micropatterned Surfaces by Cell-Dependent and -Independent Processes †. *Langmuir* 2003;19:1493–9. doi:10.1021/la026178b.
- [24] Van Vlierberghe S, Dubrue P, Schacht E. Biopolymer-based hydrogels as scaffolds for tissue engineering applications: a review. *Biomacromolecules* 2011;12:1387–408. doi:10.1021/bm200083n.
- [25] Brandl F, Sommer F, Goepferich A. Rational design of hydrogels for tissue engineering: impact of physical factors on cell behavior. *Biomaterials* 2007;28:134–46. doi:10.1016/j.biomaterials.2006.09.017.
- [26] Bashur CA, Dahlgren LA, Goldstein AS. Effect of fiber diameter and orientation on fibroblast morphology and proliferation on electrospun poly(D,L-lactic-co-glycolic acid) meshes. *Biomaterials* 2006;27:5681–8. doi:10.1016/j.biomaterials.2006.07.005.



- [27] Cooper JA, Lu HH, Ko FK, Freeman JW, Laurencin CT. Fiber-based tissue-engineered scaffold for ligament replacement: design considerations and in vitro evaluation. *Biomaterials* 2005;26:1523–32. doi:10.1016/j.biomaterials.2004.05.014.
- [28] Venugopal J, Ma LL, Yong T, Ramakrishna S. In vitro study of smooth muscle cells on polycaprolactone and collagen nanofibrous matrices. *Cell Biol Int* 2005;29:861–7. doi:10.1016/j.cellbi.2005.03.026.
- [29] Mo X., Xu C., Kotaki M, Ramakrishna S. Electrospun P(LLA-CL) nanofiber: a biomimetic extracellular matrix for smooth muscle cell and endothelial cell proliferation. *Biomaterials* 2004;25:1883–90. doi:10.1016/j.biomaterials.2003.08.042.
- [30] Yang F, Murugan R, Wang S, Ramakrishna S. Electrospinning of nano / micro scale poly ( L - lactic acid ) aligned fibers and their potential in neural tissue engineering. *Biomaterials* 2005;26:2603–10. doi:10.1016/j.biomaterials.2004.06.051.
- [31] Lee CH, Shin HJ, Cho IH, Kang Y-M, Kim IA, Park K-D, et al. Nanofiber alignment and direction of mechanical strain affect the ECM production of human ACL fibroblast. *Biomaterials* 2005;26:1261–70. doi:10.1016/j.biomaterials.2004.04.037.
- [32] Nain AS, Phillippi J a, Sitti M, Mackrell J, Campbell PG, Amon C. Control of cell behavior by aligned micro/nanofibrous biomaterial scaffolds fabricated by spinneret-based tunable engineered parameters (STEP) technique. *Small* 2008;4:1153–9. doi:10.1002/sml.200800101.
- [33] Sheets K, Wunsch S, Ng C, Nain AS. Shape-dependent cell migration and focal adhesion organization on suspended and aligned nanofiber scaffolds. *Acta Biomater* 2013;9:7169–77. doi:10.1016/j.actbio.2013.03.042.
- [34] Yoshimoto H, Shin YM, Terai H, Vacanti JP. A biodegradable nanofiber scaffold by electrospinning and its potential for bone tissue engineering. *Biomaterials* 2003;24:2077–82. doi:10.1016/S0142-9612(02)00635-X.
- [35] Barnes CP, Sell SA, Boland ED, Simpson DG, Bowlin GL. Nanofiber technology: designing the next generation of tissue engineering scaffolds. *Adv Drug Deliv Rev* 2007;59:1413–33. doi:10.1016/j.addr.2007.04.022.
- [36] Li D, Xia Y. Electrospinning of Nanofibers: Reinventing the Wheel? *Adv Mater* 2004;16:1151–70. doi:10.1002/adma.200400719.
- [37] Katta P, Alessandro M, Ramsier RD, Chase GG. Continuous Electrospinning of Aligned Polymer Nanofibers onto a Wire Drum Collector. *Nano Lett* 2004;4:2215–8. doi:10.1021/nl0486158.
- [38] Zussman E, Theron A, Yarin AL. Formation of nanofiber crossbars in electrospinning. *Appl Phys Lett* 2003;82:973–5. doi:10.1063/1.1544060.
- [39] Theron A, Zussman E, Yarin A. Electrostatic field-assisted alignment of electrospun nanofibres. *Nanotechnology* 2001;12:384–90.

- [40] Shalumon KT, Sathish D, Nair S V., Chennazhi KP, Tamura H, Jayakumar R. Fabrication of Aligned Poly(Lactic Acid)-Chitosan Nanofibers by Novel Parallel Blade Collector Method for Skin Tissue Engineering. *J Biomed Nanotechnol* 2012;8:405–16. doi:10.1166/jbn.2012.1395.
- [41] Dalton PD, Joergensen NT, Groll J, Moeller M. Patterned melt electrospun substrates for tissue engineering. *Biomed Mater* 2008;3:034109. doi:10.1088/1748-6041/3/3/034109.
- [42] Bisht GS, Canton G, Mirsepassi A, Kulinsky L, Oh S, Dunn-Rankin D, et al. Controlled continuous patterning of polymeric nanofibers on three-dimensional substrates using low-voltage near-field electrospinning. *Nano Lett* 2011;11:1831–7. doi:10.1021/nl2006164.
- [43] Sun D, Chang C, Li S, Lin L. Near-field electrospinning. *Nano Lett* 2006;6:839–42. doi:10.1021/nl0602701.
- [44] Nain AS, Wong JC, Amon C, Sitti M. Drawing suspended polymer micro-/nanofibers using glass micropipettes. *Appl Phys Lett* 2006;89:183105.
- [45] Nain AS, Amon C, Sitti M. Proximal Probes Based Nanorobotic Drawing of Polymer Micro/Nanofibers. *IEEE Trans Nanotechnol* 2006;5:499–510.
- [46] Wang J, Nain AS. Suspended micro/nanofiber hierarchical biological scaffolds fabricated using non-electrospinning STEP technique. *Langmuir* 2014;30:13641–9. doi:10.1021/la503011u.
- [47] Nain AS, Wang J. Polymeric nanofibers: isodiametric design space and methodology for depositing aligned nanofiber arrays in single and multiple layers. *Polym J* 2013;45:695–700. doi:10.1038/pj.2013.1.
- [48] *Cell Biology of Extracellular Matrix*. Springer; 1991.
- [49] Bisht GS, Canton G, Mirsepassi A, Kulinsky L, Oh S, Dunn-Rankin D, et al. Controlled continuous patterning of polymeric nanofibers on three-dimensional substrates using low-voltage near-field electrospinning. *Nano Lett* 2011;11:1831–7. doi:10.1021/nl2006164.
- [50] Chang C, Limkrailassiri K, Lin L. Continuous near-field electrospinning for large area deposition of orderly nanofiber patterns. *Appl Phys Lett* 2008;93:123111. doi:10.1063/1.2975834.
- [51] Nain AS, Wang J. Polymeric nanofibers: isodiametric design space and methodology for depositing aligned nanofiber arrays in single and multiple layers. *Polym J* 2013;45:695–700. doi:10.1038/pj.2013.1.
- [52] Wang N, Ostuni E, Whitesides GM, Ingber DE. Micropatterning tractional forces in living cells. *Cell Motil Cytoskeleton* 2002;52:97–106. doi:10.1002/cm.10037.
- [53] Wang P-Y, Yu H-T, Tsai W-B. Modulation of alignment and differentiation of skeletal myoblasts by submicron ridges/grooves surface structure. *Biotechnol Bioeng* 2010;106:285–94. doi:10.1002/bit.22697.
- [54] Stevens MM, George JH. Exploring and engineering the cell surface interface. *Science* 2005;310:1135–8. doi:10.1126/science.1106587.

- [55] Chen CS. Geometric Control of Cell Life and Death. *Science* (80- ) 1997;276:1425–8. doi:10.1126/science.276.5317.1425.
- [56] Chen CS, Mrksich M, Huang S, Whitesides GM, Ingber DE. Micropatterned surfaces for control of cell shape, position, and function. *Biotechnol Prog* n.d.;14:356–63. doi:10.1021/bp980031m.
- [57] Ji Y, Ghosh K, Zheng X, Li B, Sokolov JC, Prestwich GD, et al. Electrospun three-dimensional hyaluronic acid nanofibrous scaffolds. *Biomaterials* 2006;27:3782–92. doi:10.1016/j.biomaterials.2006.02.037.
- [58] Pham QP, Sharma U, Mikos AG. Electrospun poly(epsilon-caprolactone) microfiber and multilayer nanofiber/microfiber scaffolds: characterization of scaffolds and measurement of cellular infiltration. *Biomacromolecules* 2006;7:2796–805. doi:10.1021/bm060680j.
- [59] Erisken C, Zhang X, Moffat KL, Levine WN, Lu HH. Scaffold Fiber Diameter Regulates Human Tendon Fibroblast Growth and Differentiation. *Tissue Eng Part A* 2012;19. doi:10.1089/ten.tea.2012.0072.
- [60] Bakhru S, Nain AS, Highley C, Wang J, Campbell P, Amon C, et al. Direct and cell signaling-based, geometry-induced neuronal differentiation of neural stem cells. *Integr Biol (Camb)* 2011;1207–14. doi:10.1039/c1ib00098e.
- [61] Ker EDF, Nain AS, Weiss LE, Wang J, Suhan J, Amon CH, et al. Bioprinting of growth factors onto aligned sub-micron fibrous scaffolds for simultaneous control of cell differentiation and alignment. *Biomaterials* 2011;32:8097–107.
- [62] Nain AS, Phillippi JA, Sitti M, Mackrell J, Campbell PG, Amon C. Control of cell behavior by aligned micro/nanofibrous biomaterial scaffolds fabricated by spinneret-based tunable engineered parameters (STEP) technique. *Small* 2008;4:1153–9. doi:10.1002/smll.200800101.
- [63] Baldwin DF, Park CB, Suh NP. An extrusion system for the processing of microcellular polymer sheets: Shaping and cell growth control. *Polym Eng Sci* 1996;36:1425–35. doi:10.1002/pen.10537.
- [64] Dike LE, Chen CS, Mrksich M, Tien J, Whitesides GM, Ingber DE. Geometric control of switching between growth, apoptosis, and differentiation during angiogenesis using micropatterned substrates. *In Vitro Cell Dev Biol Anim* 1999;35:441–8. doi:10.1007/s11626-999-0050-4.
- [65] Nagasaki A, Kanada M, Uyeda TQ. Cell adhesion molecules regulate contractile ring-independent cytokinesis in *Dictyostelium discoideum*. *Cell Res* 2009;19:236–46. doi:10.1038/cr.2008.318.
- [66] Ridley AJ, Schwartz MA, Burridge K, Firtel RA, Ginsberg MH, Borisy G, et al. Cell migration: integrating signals from front to back. *Science* 2003;302:1704–9. doi:10.1126/science.1092053.
- [67] Berginski ME, Vitriol EA, Hahn KM, Gomez SM. High-resolution quantification of focal adhesion spatiotemporal dynamics in living cells. *PLoS One* 2011;6:e22025. doi:10.1371/journal.pone.0022025.

- [68] Diener A, Nebe B, Lüthen F, Becker P, Beck U, Neumann HG, et al. Control of focal adhesion dynamics by material surface characteristics. *Biomaterials* 2005;26:383–92. doi:10.1016/j.biomaterials.2004.02.038.
- [69] Dahl KN, Ribeiro AJS, Lammerding J. Nuclear shape, mechanics, and mechanotransduction. *Circ Res* 2008;102:1307–18. doi:10.1161/CIRCRESAHA.108.173989.
- [70] McBride SH, Knothe Tate ML. Modulation of stem cell shape and fate A: the role of density and seeding protocol on nucleus shape and gene expression. *Tissue Eng Part A* 2008;14:1561–72. doi:10.1089/ten.tea.2008.0112.
- [71] Bissell MJ, Weaver VM, Lelievre SA, Wang F, Petersen OW, Schmeichel KL. Tissue Structure, Nuclear Organization, and Gene Expression in Normal and Malignant Breast. *Cancer Res* 1999;59:1757s – 1764.
- [72] Brunet A, Roux D, Lenormand P, Dowd S, Keyse S, Pouyssegur J. Nuclear translocation of p42/p44 mitogen-activated protein kinase is required for growth factor-induced gene expression and cell cycle entry. *EMBO J* 1999;18:664–74. doi:10.1093/emboj/18.3.664.
- [73] Munevar S, Wang Y, Dembo M. Traction Force Microscopy of Migrating Normal and H-ras Transformed 3T3 Fibroblasts. *Biophys J* 2001;80:1744–57. doi:10.1016/S0006-3495(01)76145-0.
- [74] Du Roure O, Saez A, Buguin A, Austin RH, Chavrier P, Silberzan P, et al. Force mapping in epithelial cell migration. *Proc Natl Acad Sci U S A* 2005;102:2390–5. doi:10.1073/pnas.0408482102.
- [75] Ghibaudo M, Saez A, Trichet L, Xayaphoummine A, Browaeys J, Silberzan P, et al. Traction forces and rigidity sensing regulate cell functions. *Soft Matter* 2008;4:1836. doi:10.1039/b804103b.
- [76] Tan JL, Tien J, Pirone DM, Gray DS, Bhadriraju K, Chen CS. Cells lying on a bed of microneedles: an approach to isolate mechanical force. *Proc Natl Acad Sci U S A* 2003;100:1484–9. doi:10.1073/pnas.0235407100.
- [77] Cuenot S, Frétiigny C, Demoustier-Champagne S, Nysten B. Surface tension effect on the mechanical properties of nanomaterials measured by atomic force microscopy. *Phys Rev B* 2004;69:165410. doi:10.1103/PhysRevB.69.165410.
- [78] Discher DE, Janmey P, Wang YL. Tissue cells feel and respond to the stiffness of their substrate. *Science (80- )* 2005;310:1139–43. doi:10.1126/science.1116995.
- [79] Zhang Y-H, Zhao C-Q, Jiang L-S, Dai L-Y. Substrate stiffness regulates apoptosis and the mRNA expression of extracellular matrix regulatory genes in the rat annular cells. *Matrix Biol* 2011;30:135–44. doi:10.1016/j.matbio.2010.10.008.

## Appendix A: Copy Right Permission from Langmuir



RightsLink®

Home

Create Account

Help



Live Chat



ACS Publications  
Most Trusted. Most Cited. Most Read.

**Title:** Suspended Micro/Nanofiber Hierarchical Biological Scaffolds Fabricated Using Non-Electrospinning STEP Technique

**Author:** Ji Wang, Amrinder S. Nain

**Publication:** Langmuir

**Publisher:** American Chemical Society

**Date:** Nov 1, 2014

Copyright © 2014, American Chemical Society

LOGIN

If you're a [copyright.com](#) user, you can login to RightsLink using your [copyright.com](#) credentials. Already a RightsLink user or want to [learn more?](#)

### PERMISSION/LICENSE IS GRANTED FOR YOUR ORDER AT NO CHARGE

This type of permission/license, instead of the standard Terms & Conditions, is sent to you because no fee is being charged for your order. Please note the following:

- Permission is granted for your request in both print and electronic formats, and translations.
- If figures and/or tables were requested, they may be adapted or used in part.
- Please print this page for your records and send a copy of it to your publisher/graduate school.
- Appropriate credit for the requested material should be given as follows: "Reprinted (adapted) with permission from (COMPLETE REFERENCE CITATION). Copyright (YEAR) American Chemical Society." Insert appropriate information in place of the capitalized words.
- One-time permission is granted only for the use specified in your request. No additional uses are granted (such as derivative works or other editions). For any other uses, please submit a new request.

## Appendix B: Copy Right Permission from Polymer Journal Nature



RightsLink®

Home

Create Account

Help



**Title:** Polymeric nanofibers: isodiametric design space and methodology for depositing aligned nanofiber arrays in single and multiple layers

**Author:** Amrinder S Nain and Ji Wang

**Publication:** Polymer Journal

**Publisher:** Nature Publishing Group

**Date:** Feb 13, 2013

Copyright © 2013, Rights Managed by Nature Publishing Group

**LOGIN**  
If you're a [copyright.com](#) user, you can login to RightsLink using your [copyright.com](#) credentials. Already a [RightsLink](#) user or want to [learn more?](#)

### Author Request

If you are the author of this content (or his/her designated agent) please read the following. If you are not the author of this content, please click the Back button and select an alternative [Requestor Type](#) to obtain a quick price or to place an order.

Ownership of copyright in the article remains with the Authors, and provided that, when reproducing the Contribution or extracts from it, the Authors acknowledge first and reference publication in the Journal, the Authors retain the following non-exclusive rights:

- a) To reproduce the Contribution in whole or in part in any printed volume (book or thesis) of which they are the author(s).
- b) They and any academic institution where they work at the time may reproduce the Contribution for the purpose of course teaching.
- c) To reuse figures or tables created by them and contained in the Contribution in other works created by them.